



# An evaluation of ozone dry deposition in global scale chemistry climate models

C. Hardacre<sup>1</sup>, O. Wild<sup>1</sup>, and L. Emberson<sup>2</sup>

<sup>1</sup>Lancaster Environment Centre, Lancaster University, Lancaster, UK

<sup>2</sup>Stockholm Environment Institute, University of York, York, UK

Correspondence to: O. Wild (o.wild@lancaster.ac.uk)

Received: 10 July 2014 – Published in Atmos. Chem. Phys. Discuss.: 8 September 2014

Revised: 30 April 2015 – Accepted: 11 May 2015 – Published: 12 June 2015

**Abstract.** Dry deposition to the Earth's surface is an important process from both an atmospheric and biospheric perspective. Dry deposition controls the atmospheric abundance of many compounds as well as their input to vegetative surfaces, thus linking the atmosphere and biosphere. In many atmospheric and Earth system models it is represented using “resistance in series” schemes developed in the 1980s. These methods have remained relatively unchanged since their development and do not take into account more recent understanding of the underlying processes that have been gained through field and laboratory based studies. In this study we compare dry deposition of ozone across 15 models which contributed to the TF HTAP model intercomparison to identify where differences occur. We compare modelled dry deposition of ozone to measurements made at a variety of locations in Europe and North America, noting differences of up to a factor of two but no clear systematic bias over the sites examined. We identify a number of measures that are needed to provide a more critical evaluation of dry deposition fluxes and advance model development.

and Ehhalt, 2001) and is also a potent pollutant in its own right (The Royal Society, 2008).

Elevated concentrations of O<sub>3</sub> in the troposphere are detrimental to the human respiratory system and to plant health (e.g. WHO, 2005; Ashmore, 2005; The Royal Society, 2008; Fowler et al., 2009; Anenberg et al., 2010; Ainsworth et al., 2012; Emberson et al., 2013; Simpson et al., 2014) as it is a strong oxidant. Anenberg et al. (2010) estimated that anthropogenic O<sub>3</sub> pollution was associated with  $0.7 \pm 0.3$  million global deaths annually in the year 2000. It also has impacts on global agricultural production (Van Dingenen et al., 2009; Avnery et al., 2011a, b), with losses from three major crops estimated to be USD<sub>2000</sub> 11–18 billion annually in the year 2000 (Avnery et al., 2011a) and projected to rise to USD<sub>2000</sub> 12–35 billion in the year 2030 (Avnery et al., 2011b). However, the role of O<sub>3</sub> in future climate scenarios is not straightforward. The effect of O<sub>3</sub> on crop production between 2000 and 2050 may either exacerbate or offset the effects of climate change depending on scenario, crop type and region (Tai et al., 2014).

Ozone is primarily removed from the troposphere by chemical destruction and dry deposition to the Earth's surface. Dry deposition processes account for about 25 % of the total O<sub>3</sub> removed from the troposphere (Lelieveld and Dentener, 2000). Because it occurs at the Earth's surface–atmosphere interfaces, dry deposition constrains both the near-surface O<sub>3</sub> concentration and the input of O<sub>3</sub> to surface ecosystems. In rural areas, dry deposition to terrestrial surfaces drives the diurnal variation in surface O<sub>3</sub> (Simpson, 1992). Further, for a reactive and polluting compound such as ozone, understanding dry deposition processes is particularly important for assessing impacts on terrestrial ecosys-

## 1 Introduction

Ozone is a significant trace gas constituent in the troposphere. The two main sources of tropospheric ozone are transport from the stratosphere and in situ chemical production via the oxidation of hydrocarbons and CO in the presence of nitrogen oxides (NO<sub>x</sub>) (Crutzen, 1974; Liu et al., 1980; Atkinson, 2000). Tropospheric O<sub>3</sub>, in addition to being a greenhouse gas, is the primary driver of chemical oxidation in the troposphere as a source of OH radicals (e.g. Prather

tems where O<sub>3</sub>-induced damage to vegetation may affect the hydrological cycle and key biogeochemical cycles, including those of carbon and nitrogen.

Dry deposition of O<sub>3</sub> to the terrestrial Earth surface is highly dependent on land cover. Deposition to non-vegetated surfaces is generally slower than deposition to vegetated surfaces (Wesely and Hicks, 2000) and the latter process varies according to plant species and seasonal changes in leaf area index (LAI). At vegetated surfaces, 30–90 % of O<sub>3</sub> dry deposition occurs via the stomata (Fowler et al., 2001; Cieslik, 2004; Fowler et al., 2009) and is controlled by stomatal conductance, which varies according to species and meteorological conditions. It is uptake of O<sub>3</sub> through the stomata that results in damage to plant tissues, which are subsequently exposed to the highly reactive O<sub>3</sub>, negatively impacting plant health (e.g. Reich and Amundson, 1985; Fowler et al., 2001).

The strong link between dry deposition, the atmosphere and land cover means that this process is also subject to feedbacks from changes in climate, land use and air pollution (Ainsworth et al., 2012; Fuhrer, 2009; Sitch et al., 2007; Arneeth et al., 2010; Ganzeveld et al., 2010; Wu et al., 2012; Hollaway, 2012; Hardacre et al., 2013). For example, increasing atmospheric CO<sub>2</sub> has been shown to affect tropospheric O<sub>3</sub> as a result of changes in stomatal conductance (Sitch et al., 2007). However, despite the importance of dry deposition processes, they are some of the most uncertain and poorly constrained aspects of the tropospheric O<sub>3</sub> budget (Wild, 2007). This uncertainty arises from the complexity and heterogeneity in dry deposition processes which depend on meteorological conditions and the characteristics of the surface, along with a paucity of long term observation data sets for many surface cover classes, including oceans, tropical forests and deserts.

Global chemistry transport models (CTMs) or chemistry climate models (CCMs) are needed to study O<sub>3</sub> at a global scale. Uncertainty in dry deposition arises partly from it occurring at sub-grid scales and because the process is heavily parameterized in models (Giannakopoulos et al., 1999; Wesely and Hicks, 2000; Fowler et al., 2009). The global O<sub>3</sub> dry deposition sink is estimated from a wide range of modelling studies to be about 1000 Tg yr<sup>-1</sup> (Stevenson et al., 2006; Wild, 2007; Young et al., 2013). Of this, approximately one third is deposited to the oceans (Ganzeveld et al., 2009).

Many global scale CTMs parameterize dry deposition using the resistance in series approach developed by Wesely (1989) with some modifications (e.g. Wang et al., 1998; Ganzeveld and Lelieveld, 1995; Val Martin et al., 2014). This scheme is well characterized and has been previously reviewed, e.g. by Wesely and Hicks (2000) and Fowler et al. (2009). The Wesely scheme does not, however, take into account newer understanding of dry deposition processes that has been gained from more recent measurement studies. Notably, the importance of surface wetness, soil moisture, vapour pressure deficit and the role of stomatal versus non-stomatal uptake have been clearly demonstrated (Fowler

et al., 2009). The latter is of particular importance for assessing the impact of O<sub>3</sub> on plants, as it is the uptake of O<sub>3</sub> through the stomata that results in damage to plant tissues.

Comparatively recent process models such as DO3SE (Emberson et al., 2000b, a, 2001; Buker et al., 2007), which was developed to estimate stomatal ozone flux, do parameterize the effect of soil water deficit and vapour pressure deficit on stomatal conductance. DO3SE has recently been included in the EMEP model (Simpson et al., 2012), but these developments have not generally been implemented in global scale models.

In this study we conduct the first global scale assessment of O<sub>3</sub> dry deposition across a wide range of CTMs and CCMs. While dry deposition has been studied in detail in individual models (e.g. Tuovinen et al., 2004, 2009; Zhang et al., 2002), no general comparative evaluation has been performed across a wider range of models to explore model differences or weaknesses. Here, we identify the main differences between models and highlight the diagnostics that would be required from future studies to provide better constraints on O<sub>3</sub> dry deposition at the global scale. We use O<sub>3</sub> dry deposition fluxes from a subset of 15 models that contributed to the model intercomparison coordinated by the Task Force on Hemispheric Transport of Air Pollution (TF HTAP) (Fiore et al., 2009). Results from these models have been used to study nitrogen and sulfur deposition (Sanderson et al., 2008; Dentener et al., 2006) as well as tropospheric ozone (Stevenson et al., 2006) at the global scale, but an assessment of ozone dry deposition has not previously been undertaken.

We describe the methods used to process the model data in Sect. 2. The analysis of modelled O<sub>3</sub> dry deposition is shown in Sects. 3.1 and 3.2. We analyse O<sub>3</sub> deposition fluxes partitioned to land cover classes to evaluate the driving factors for variation in O<sub>3</sub> dry deposition that are associated with land cover across the model ensemble in Sect. 4. Finally, we compare modelled O<sub>3</sub> deposition fluxes to measurements in Sect. 5.

## 2 Methods

Ozone dry deposition fluxes were diagnosed and archived from 15 of the global chemistry transport models that participated in the TF HTAP modelling intercomparison project (for further details see <http://www.htap.org>). These models and the main differences between them are detailed in Sanderson et al. (2008), Dentener et al. (2006) and Stevenson et al. (2006). Average monthly O<sub>3</sub> dry deposition fluxes were taken from the TF HTAP control run (the “SR1 experiment”) which was driven by meteorological fields for the year 2001. Note that the diurnal variation in deposition fluxes is not available from the TF HTAP results, so we focus our analysis on monthly fluxes. The models used in this study

**Table 1.** Summary of the deposition schemes and annual total global O<sub>3</sub> dry deposition fluxes for 15 TF HTAP models.

Model	Deposition scheme <sup>a</sup>	Land cover classes <sup>b</sup>	Annual global O <sub>3</sub> deposition/Tg yr <sup>-1</sup>	Reference
CAMCHEM-3311m13	Wesely	17	861	Lamarque et al. (2012)
CAMCHEM-3514	Wesely	17	818	Lamarque et al. (2012)
CHASER-v03	Wesely		939	Sudo et al. (2002)
FRSGC/UCI-v01	Wesely	9	943	Wild and Prather (2000)
GEMAQ-EC	Wesely	15	878	Kaminski et al. (2008)
GEOSChem-v07	Wesely	11	913	Bey et al. (2001)
GISS-PUCCINI-modelA	Wesely	8	975	Shindell et al. (2001)
GISS-PUCCINI-modelEaer	Wesely	8	1112	Shindell et al. (2001)
GISS-PUCCINI-modelE	Wesely	8	1179	Shindell et al. (2001)
GMI-v02f	Wesely		819	Rotman et al. (2001)
INCA-vSSz	Wesely	11	1256	Hauglustaine et al. (2004)
LLNL-IMPACT-T5a	Wesely	13	1000	Rotman et al. (2004)
MOZARTGFDL-v2	Wesely	11	997	Horowitz et al. (2003)
STOC-HadAM3-v01	Wesely	9	1095	Collins et al. (2003)
STOCHEM-v02	Wesely	9	834	Collins et al. (1997)
TM5-JRC-cy2-ipcc-v1	Wesely	4	844	Huijnen et al. (2010)
ULAQ-v02	Prescribed <sup>c</sup>		1116	Pitari et al. (1992)
UM-CAM-v01	Prescribed <sup>c</sup>	5	1023	Zeng et al. (2003)
Average ( $\pm 1\sigma$ )			978 $\pm$ 127	
Average seasonal amplitude <sup>d</sup>			38 $\pm$ 8	
Average monthly range <sup>e</sup>			38 $\pm$ 6	

<sup>a</sup> The Wesely scheme has been updated from the original scheme (Wesely, 1989) in many of these models. Further details about these updates are given in the Supplement. <sup>b</sup> The number of land cover classes used in the model are shown here. The land cover classes are listed for each model in the Supplement. <sup>c</sup> Deposition velocities are prescribed for land cover type, season and whether it is day or night. <sup>d</sup> Defined here as the difference in total global O<sub>3</sub> dry deposition between the months with highest and lowest deposition fluxes. <sup>e</sup> Average monthly range is the average spread across the models for each month.

are summarized in Table 1 and more details on the deposition schemes and land cover are given in the Supplement.

In most of the models dry deposition of gases was represented using the resistance in series scheme described by Wesely (1989) or a modified version of this scheme. In this type of scheme the dry deposition velocity is determined from Eq. (1):

$$V_d = (R_a + R_b + R_c)^{-1}, \quad (1)$$

where the terms  $R_a$ ,  $R_b$  and  $R_c$  represent the aerodynamic resistance, quasi-laminar layer resistance and canopy surface resistance. Although this method is practical, the properties of the atmosphere and surface can be oversimplified (Wesely and Hicks, 2000). The  $R_c$  term may differ considerably between models depending on how individual surface resistance terms (e.g. stomatal resistance,  $R_{\text{stom}}$ , and mesophyll resistance,  $R_m$ ) are represented (Wesely and Hicks, 2000). The original dry deposition module developed by Wesely (1989) described seven surface resistance terms for 11 land use types and five seasonal categories, but these may be mapped to the native land cover classes in the models differently.

The horizontal resolution of the different models ranged from  $1^\circ \times 1^\circ$  to  $10^\circ \times 10^\circ$ , averaging approximately  $3^\circ \times 3^\circ$ .

Ozone dry deposition fluxes from all models were therefore regridded to a common horizontal resolution of  $3^\circ \times 3^\circ$  to enable ensemble means and standard deviations to be calculated for each grid box.

To account for first order variation in the simulated O<sub>3</sub> dry deposition fluxes arising from model differences in surface O<sub>3</sub>, dry deposition velocities were also compared. Modelled deposition velocities are not available from the TF HTAP archive, so these were calculated from Eq. (2):

$$V_d = F_{O_3}/C_{O_3}, \quad (2)$$

where  $F_{O_3}$  and  $C_{O_3}$  are the simulated dry deposition flux and surface O<sub>3</sub> concentration respectively. These mean dry deposition velocities are O<sub>3</sub>-weighted and thus do not account for diurnal variations in surface O<sub>3</sub> or O<sub>3</sub> flux, which are not available for this study, or for indirect variations in flux arising from the feedback between surface O<sub>3</sub> and its deposition, which limits the fluxes when velocities are large. However, variation as a result of these processes is likely to be small compared with the variation in surface O<sub>3</sub>.

To better characterize sources of variation in O<sub>3</sub> dry deposition between models, the fluxes were partitioned to different land cover classes (LCCs). Modelled O<sub>3</sub> dry deposition is only available as a monthly average flux per grid cell, so

it was necessary to repartition the fluxes for different land classes. The repartitioned fluxes were then used to determine deposition velocities to individual land cover classes. The land cover schemes used in the TF HTAP models differ in their degree of classification, with some schemes including as many as 17 LCCs and others as few as five. The land cover schemes from individual models were not available for this study, so we apply two common schemes to all models. Ozone dry deposition fluxes for individual LCCs were determined by summing fluxes over grid cells,  $i$ , scaled by the fractional area,  $f$ , for that land cover class,  $c$ , see Eq. (3). Total  $O_3$  deposition per LCC was determined globally over all grid cells and by latitude by summing over separate latitude bands.

$$F_c = \frac{\sum_i F_i \cdot A_i \cdot f_{i,c}}{\sum_i A_i} \quad (3)$$

The modelled  $O_3$  dry deposition fluxes were compared to observed dry deposition fluxes from several sites, primarily located in Europe and North America. Seven of these data sets covered periods of more than a year and detailed comparisons between the modelled and observed  $O_3$  dry deposition fluxes were made at these sites. Shorter term measurements were made at a number of other sites. The measurement sites are described in greater detail in Sect. 5.1.

To compare measured fluxes with the modelled average monthly  $O_3$  dry deposition fluxes we focussed on studies that reported an average  $O_3$  dry deposition flux or where long term average  $O_3$  dry deposition flux data was independently made available for this study. We focus on data sets that include a full seasonal cycle so that we can explore how well the models resolve the large contrasts in  $O_3$  dry deposition between summer and winter. We also compare the measured  $O_3$  dry deposition fluxes with modelled fluxes repartitioned for the land cover classes in the corresponding grid cell. The flux to each land cover class was determined assuming that the ratio of the fluxes in the grid cell was the same as that around the corresponding latitude band.

This approach to repartitioning fluxes for individual LCCs was tested using a single model, the FRSGC/UCI CTM (Wild and Prather, 2000), where land cover specific fluxes were explicitly diagnosed. The repartitioned fluxes were found to be in reasonable agreement with the explicitly diagnosed fluxes, typically within about 10% over the globe, and within 20% for all nine land cover classes considered. This gives an indication of the level of uncertainty associated with this simple partitioning approach.

We also compared the modelled monthly average  $O_3$  dry deposition fluxes to data from the Clean Air Status and Trends Network (CASTNET, <http://epa.gov/castnet/javaweb/index.html>). As CASTNET deposition fluxes are derived using modelled deposition velocities rather than directly measured fluxes, we discuss the results separately from our comparison with fluxes measured at European and North American sites. Hourly surface  $O_3$  measurements and

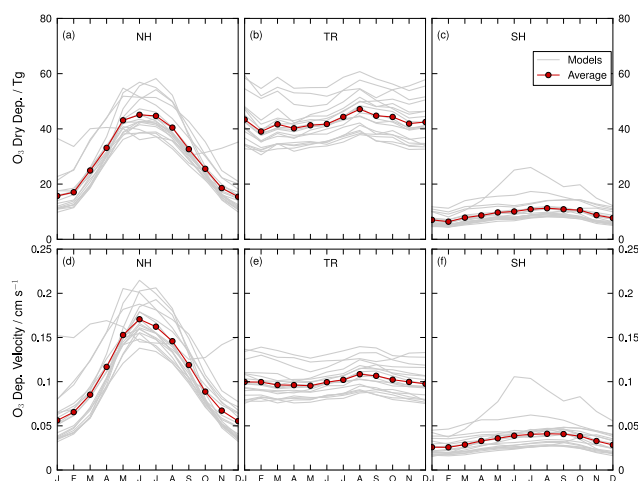


**Figure 1.** Total monthly  $O_3$  dry deposition (top, a–c) and monthly average  $O_3$  deposition velocity (bottom, d–f) for 15 models participating in the TF HTAP model intercomparison project. Modelled monthly total  $O_3$  dry deposition is shown for the Northern Hemisphere extra-Tropics 30–90° N (a, d), Tropics 30° N–30° S (b, e), and Southern Hemisphere extra-Tropics 30–90° S (c, f).

derived  $O_3$  dry deposition velocities (Clarke et al., 1997; Finkelstein et al., 2000) are available for 96 sites across North America. We determined the monthly average surface  $O_3$  and  $O_3$  deposition velocity at each site and calculated the monthly average deposition flux. The data were grouped by land cover class according to the site descriptions, and sites classified as forest, grassland, crop and shrub/desert are included here.

### 3 Results and discussion

#### 3.1 Global variation in $O_3$ dry deposition

Annual global  $O_3$  dry deposition fluxes from the 15 TF HTAP models are summarized in Table 1, and the seasonal cycles are shown in Fig. 1 for three distinct latitude bands. The modelled annual global deposition fluxes ranged between 818 and 1256  $Tg\ yr^{-1}$  across the models with an ensemble mean ( $\pm 1\sigma$ ) of  $978 \pm 127\ Tg\ yr^{-1}$ . This is very similar to that reported in previous modelling studies, including  $949 \pm 222\ Tg\ yr^{-1}$  from 17 independent studies between 2000 and 2004 (Wild, 2007),  $1003 \pm 200\ Tg\ yr^{-1}$  from 21 models contributing to the ACCENT model intercomparison (Stevenson et al., 2006) and  $1094 \pm 241\ Tg\ yr^{-1}$  from six models contributing to the recent ACCMIP intercomparison (Young et al., 2013). In these studies, 9 out of 29 models in Wild (2007), 9 out of 21 models in Stevenson et al. (2006) and 3 out of 6 models in Young et al. (2013) were similar to those used in this study.

Monthly  $O_3$  deposition varied by an average of  $38 \pm 6\ Tg\ month^{-1}$  across the model ensemble; see Table 1. On av-

average dry deposition velocities varied by  $0.09 \pm 0.02 \text{ cm s}^{-1}$  per month. The average relative standard deviations (RSDs) for total monthly dry deposition and average monthly deposition velocity are 14 % and 20 %. The smaller RSD for total monthly deposition indicates that differences in surface  $\text{O}_3$  compensate for some of the differences in  $\text{O}_3$  dry deposition velocity between the models, i.e. that the  $\text{O}_3$  deposition velocity is more different across the models than the  $\text{O}_3$  deposition flux.

The original Wesely scheme describes a limited seasonality for surface resistance with smaller resistances to vegetated surfaces in spring and summer (Wesely, 1989). In this study the models agree well on the timing of the seasonal cycles in dry deposition in the Northern Hemisphere (NH), Tropics and the Southern Hemisphere (SH) (Fig. 1). Differences in the seasonality may arise from differences in meteorology or in surface vegetation cover. The effect of the latter is discussed further in Sect. 4.

Figure 1 shows that  $\text{O}_3$  dry deposition is greatest in the Tropics and in the NH during the growing season. For all the HTAP models the most well-defined seasonal cycle in  $\text{O}_3$  dry deposition occurs in the Northern Hemisphere with maximum and minimum deposition during the NH summer and winter respectively. In contrast the seasonality in the Tropics and Southern Hemisphere is much less pronounced. The average RSD in monthly total deposition over the models (NH = 21 %, Tropics = 15 % and SH = 32 %) is smaller than the average RSD in monthly average deposition velocity in the NH (31 %), Tropics (21 %) and SH (36 %), again highlighting the compensation between surface  $\text{O}_3$  and deposition velocity between the models in these regions.

### 3.2 Latitudinal variation in $\text{O}_3$ dry deposition

The latitudinal distribution of total annual  $\text{O}_3$  dry deposition is shown for the model ensemble in Fig. 2. The  $\text{O}_3$  dry deposition is greatest between  $30^\circ \text{ S}$  and  $45^\circ \text{ N}$ , with an average flux of  $20\text{--}37 \text{ Tg yr}^{-1}$  per  $3^\circ$  latitude band, and the RSD over the models is relatively uniform at 15–20 %.

In contrast, there are greater differences in dry deposition velocity between the models. Five models show a peak in deposition velocity at  $0\text{--}15^\circ \text{ S}$ . These models included a tropical forest or broadleaf evergreen forest land cover class, but were not the only models to do so. The RSD in the dry deposition velocity was generally between 30 and 35 % at mid-latitudes.

The seasonality in the dry deposition flux is shown for February and August in Fig. 2 to highlight both the temporal and spatial variability in deposition. In February,  $\text{O}_3$  dry deposition is greatest at  $0\text{--}30^\circ \text{ N}$ , driven by higher surface  $\text{O}_3$  and LAI in this region, and the deposition velocities are fairly uniform between  $30^\circ \text{ N}$  and  $30^\circ \text{ S}$ . In August, peak deposition shifts northward to  $30\text{--}45^\circ \text{ N}$ , but peak dry deposition velocities occur further north, (approx.  $55\text{--}65^\circ \text{ N}$ ), further indicating that high summertime  $\text{O}_3$  dry deposition in

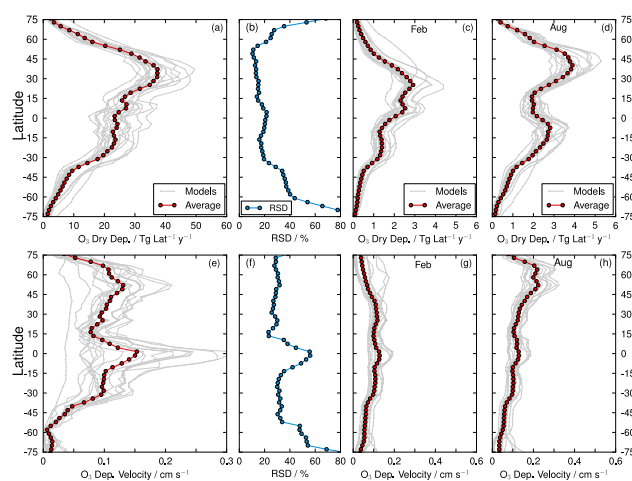


**Figure 2.** Latitudinal distribution of total  $\text{O}_3$  dry deposition (top row) and average  $\text{O}_3$  deposition velocities (bottom row) per  $3^\circ$  latitude band for the model ensemble. Panels show the total annual  $\text{O}_3$  dry deposition and average annual  $\text{O}_3$  dry deposition velocity (a, e), the relative standard deviation (RSD) in annual deposition and average annual deposition velocity across the models (b, f), and the total monthly  $\text{O}_3$  dry deposition fluxes and average annual dry deposition velocities in February (c, g) and August (d, h).

the NH is driven by both increased LAI in the growing season and by high summertime surface  $\text{O}_3$  (Stevenson et al., 2006; Fiore et al., 2009; Young et al., 2013). A second peak in  $\text{O}_3$  deposition, also mainly driven by high surface  $\text{O}_3$ , occurs at  $0\text{--}30^\circ \text{ S}$  and is associated with dry deposition to deciduous trees and grassland.

### 4 $\text{O}_3$ dry deposition to different land cover classes

The greatest variation in  $\text{O}_3$  dry deposition occurs between  $45^\circ \text{ N}$  and  $30^\circ \text{ S}$ , i.e. where vegetated terrestrial land cover is primarily located. To investigate how land cover contributes to variation in  $\text{O}_3$  dry deposition across the model ensemble, the fluxes were partitioned to different land cover classes (LCCs) as described in Sect. 2.

Because the native land cover schemes used in the TF HTAP models are not available for this study, data from Olson 1992 (available though: <http://acmg.seas.harvard.edu/geos/>, Loveland et al., 2000) and the Global Land Cover Facility (GLCF, available from <http://www.landcover.org/>, De Fries and Townshend, 1994) are used. This results in some additional uncertainty in the partitioned fluxes, particularly in regions where landcover is very heterogeneous. However, by using two different land cover schemes for partitioning fluxes across the model ensemble, we gain a clearer picture of the sensitivity of simulated  $\text{O}_3$  dry deposition to land cover.

The Olson 1992 data set describes fractional grid cell coverage for 74 LCCs at  $1^\circ \times 1^\circ$  resolution. These 74 LCCs were



**Table 2.** Land cover classification for the OW11 and GLCF data sets.

Land cover class		Abbreviation		% area	
OW11	GLCF	OW11	GLCF	OW11	GLCF
Snow and ice	Snow and ice	SI	SI	2.7	3.5
Deciduous forest	Broadleaf deciduous forest	DF	BD	4.9	0.7
–	High-latitude deciduous forest	–	HL	–	1.2
Coniferous forest	Coniferous evergreen forest	CF	CE	3.1	2.5
–	Mixed coniferous forest and woodland	–	MC	–	1.4
Agricultural land, crops	Crops	AC	CR	2.7	3.1
Grassland	Grassland	GL	GL	8.2	4.3
–	Wooded grassland	–	WG	–	4.7
Tropical forest	Broadleaf evergreen forest	TF	BE	0.8	2.9
Tundra	Tundra	TN	TN	1.7	1.5
Desert	Bare ground	DT	BG	3.8	3.4
–	Shrubs, bare ground	–	SB	–	2.1
Wetland	–	WL	–	0.7	–
Urban	–	UB	–	0.0	–
Water	Water	WT	WT	71.2	68.6
Total				100	100

mapped to the 11 Wesely LCCs described in Table 2. The resulting land cover data set is henceforth termed the “OW11” data set. The GLCF data set describes grid cell coverage for 14 LCCs at  $1^\circ \times 1^\circ$  resolution, but provides only the dominant LCC at the  $1^\circ \times 1^\circ$  scale. Both data sets were regridded to the same  $3^\circ \times 3^\circ$  resolution as the model output. The OW11 and GLCF LCCs and their global coverage are summarized in Table 2.

#### 4.1 Variation in $O_3$ dry deposition fluxes at homogeneous grid cell locations

Variation in  $O_3$  dry deposition velocity to individual LCCs was initially compared at  $3^\circ$  grid cells that were dominated by a single land cover class in the OW11 data set. Monthly  $O_3$  dry deposition velocities were averaged over all grid cells with 100 % coverage of a single LCC. Maps of these grid cells are provided in the Supplement. In taking this approach, we remove some of the uncertainty associated with using non-native land cover data, as models are likely to be reasonably consistent in their land cover across these regions. This analysis reveals the variability in  $O_3$  dry deposition velocities to different LCCs across the ensemble. Urban and wetland LCCs were not considered here as their global coverage is small (see Table 2).

Figure 3 shows that seasonality in  $O_3$  dry deposition velocities for the terrestrial vegetated LCCs agree well across the model ensemble. The only exception is one coarse resolution model which did not include any seasonal variation in  $O_3$  dry deposition. The magnitude of the dry deposition velocities varies by  $0.002$ – $0.25 \text{ cm s}^{-1}$  across the model ensemble, with greatest variation occurring during the NH growing season for all terrestrial vegetated LCCs except tropical

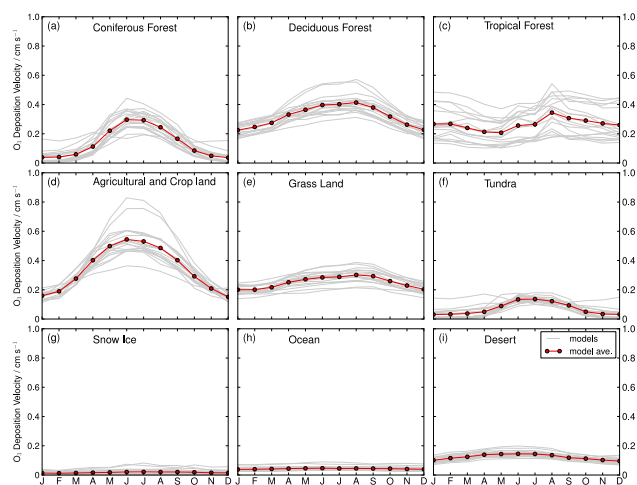


**Figure 3.** Average monthly  $O_3$  dry deposition velocities at grid cells with 100 % coverage of a given land cover class. Model deposition velocities are shown in grey and the ensemble average in red.

forest. Variation in  $O_3$  dry deposition to tropical forest was not seasonal, averaging about  $0.3 \text{ cm s}^{-1}$  throughout the year (see Fig. 3c). At non-vegetated LCCs (oceans, snow/ice and deserts) the variation in  $O_3$  dry deposition velocity across the ensemble was small.

The absence of seasonal variation in  $O_3$  dry deposition velocity to tropical forests was likely due to relatively uniform annual LAI compared to other LCCs, such as coniferous forest, deciduous forest, agricultural cropland and tundra, where there are large differences in LAI between the growing and non-growing seasons. Different representation of LAI across the models is therefore likely to drive part of the observed

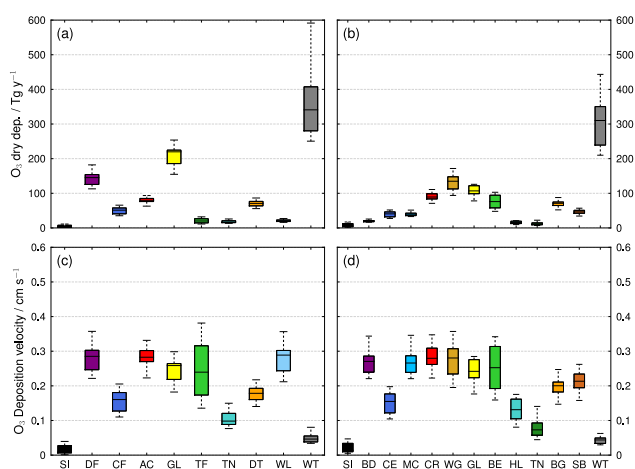


**Figure 4.** Total annual  $\text{O}_3$  dry deposition and annual average  $\text{O}_3$  deposition velocity partitioned to land cover classes using the OW11 (a, c) and GCLF (b, d) data sets. Upper panels show the contribution of each LCC to the global annual  $\text{O}_3$  dry deposition flux, and lower panels show the average deposition velocity to each LCC. The box and whiskers for each land class represent the median, quartiles and 10th/90th percentiles over the 15 contributing models.

greater spread in  $\text{O}_3$  dry deposition over the models during the NH growing season for coniferous forest, deciduous forest, agricultural cropland and tundra.

For deciduous forest and agricultural cropland high summertime  $\text{O}_3$  dry deposition velocities were observed for two models. These models may either specify relatively high deposition velocities to these land cover classes, or classify and distribute land cover very differently to the other models. Diagnosing land cover specific dry deposition fluxes and velocities would allow for a more detailed analysis of the drivers of these differences between models.

#### 4.2 Variation in total $\text{O}_3$ dry deposition to land cover classes

Figure 4 shows the total  $\text{O}_3$  deposition to LCCs described in the OW11 and GCLF land cover data sets. The largest total flux of  $\text{O}_3$  is to the oceans, which remove an average of  $361 \text{ Tg O}_3 \text{ yr}^{-1}$ , and this is followed by grasslands and deciduous trees which remove  $207$  and  $142 \text{ Tg O}_3 \text{ yr}^{-1}$  respectively, based on fluxes partitioned to the OW11 data set. Partitioning to the GCLF data set gives a broadly similar picture, with oceans, wooded grassland and grassland responsible for fluxes of  $319$ ,  $131$  and  $107 \text{ Tg O}_3 \text{ yr}^{-1}$  respectively.

Deciduous forest is not classified uniquely in the GCLF data set, and the corresponding area is predominantly considered as wooded grassland, broad leaf evergreen forest and broad leaf deciduous forest. The greater average  $\text{O}_3$  dry deposition to broad leaf evergreen forest (BE) compared with tropical forest,  $75$  and  $20 \text{ Tg O}_3 \text{ yr}^{-1}$  respectively, reflects the larger area for BE than tropical forest in OW11 (see Table 2).

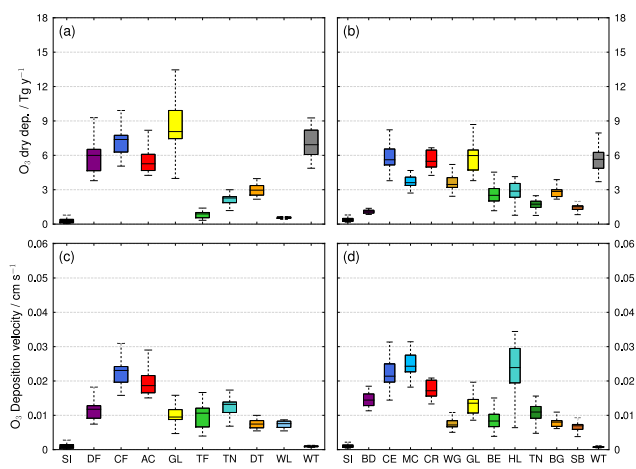
The average flux to other LCCs, e.g. crops and coniferous forest, was broadly similar for the two land cover data sets.

Figure 4 clearly shows that total global  $\text{O}_3$  deposited to oceans is both large and highly variable across the different models. Deposition to oceans is  $250$ – $591 \text{ Tg yr}^{-1}$  using the OW11 data set ( $209$ – $538 \text{ Tg yr}^{-1}$  using the GCLF data set), representing a range of about  $335 \text{ Tg yr}^{-1}$  across the ensemble. The geographical distribution of  $\text{O}_3$  dry deposition fluxes to the oceans indicates that differences between the models are spatially uniform. The range in total  $\text{O}_3$  deposition to the other LCCs that are large  $\text{O}_3$  sinks, e.g. deciduous trees and grassland (OW11) and wooded grassland and BE (GCLF), is  $70$ – $100 \text{ Tg yr}^{-1}$ .

The lower panels in Fig. 4 show that the variation in the average deposition velocity to oceans is small in absolute terms,  $< 0.1 \text{ cm s}^{-1}$ . However, integrating these small differences over the large global area of ocean leads to large differences in total deposition. The sensitivity of surface  $\text{O}_3$  to small variations in dry deposition velocity over the oceans was also reported by Ganzeveld et al. (2009), who found that surface  $\text{O}_3$  differed by up to 60 % when the  $\text{O}_3$  dry deposition velocity was varied between  $0.01$  and  $0.05 \text{ cm s}^{-1}$ . Improved characterization of deposition velocities over the ocean, building on the work of Ganzeveld et al. (2009) and Helmig et al. (2012), would therefore make a substantial contribution to reducing the uncertainty in total global  $\text{O}_3$  dry deposition. Further, it is important to constrain the absolute deposition velocities for other LCCs that cover a large area, e.g. for grassland, and to describe spatial variation in  $\text{O}_3$  dry deposition better, e.g. with more descriptive land cover data sets.

Model differences are particularly evident for tropical forest, where the range in average  $\text{O}_3$  dry deposition velocity is  $0.25 \text{ cm s}^{-1}$ . Tropical forest is not explicitly defined in some of the models used in this study, or in the original Wesely scheme, so it is apparent that a range of  $\text{O}_3$  deposition velocities have been applied in these areas across the models. This has less impact for the  $\text{O}_3$  dry deposition budget using the OW11 data set, where the tropical forest area is relatively small, but is a larger source of uncertainty when using the GCLF data set. It is important to include a well-constrained  $\text{O}_3$  dry deposition velocity and global area for tropical forests as observed mean daytime maximum velocities of  $2.3 \text{ cm s}^{-1}$  (Rummel et al., 2007) suggest that they are an effective  $\text{O}_3$  sink.

This comparison highlights the importance of well-constrained  $\text{O}_3$  deposition velocities, particularly over water where small differences result in large discrepancies in total  $\text{O}_3$  deposition, but also to tropical forests. The importance of land cover classification within models is also emphasized. The differences in fluxes to tropical forests could be greatly reduced by including a specific  $\text{O}_3$  deposition velocity for this LCC. The LCC distribution is also shown to be important. For example, the tropical forest and broadleaf evergreen LCCs in the OW11 and GCLF data sets cover  $0.8$  and  $2.9$  % respectively, partly as a result of the use of dominant veg-



**Figure 5.** Seasonal amplitude in total global  $\text{O}_3$  dry deposition partitioned to the OW11 (a) and GCLF (b) land cover classes. The monthly range in average  $\text{O}_3$  dry deposition velocity is shown in the lower panels for OW11 (c) and GCLF (d) land cover classes. The box and whiskers represent the median, quartiles and 10th/90th percentiles over the model ensemble.

etation types at scale in the latter data set. A high  $\text{O}_3$  dry deposition velocity over these two areas would yield different total deposition and could have very different impacts on local atmospheric chemistry and composition.

### 4.3 Seasonal variation in $\text{O}_3$ dry deposition to land cover classes

The differences in total  $\text{O}_3$  dry deposition between the months with highest and lowest deposition, representing the seasonal amplitude, are shown in Fig. 5. The largest seasonal amplitudes are found for deciduous forests, coniferous forests, agricultural crop land, grassland and water in the OW11 data set. Similarly, they are found for coniferous evergreen (CE), mixed coniferous forest (MC), crop land, grassland, high latitude deciduous forest and woodland (HL) and oceans in the GCLF data set.

These differences in the seasonal amplitude of deposition to coniferous, agricultural and high latitude LCCs in both data sets are driven by differences in the seasonal amplitude in  $\text{O}_3$  deposition velocity, shown in the lower panels of Fig. 5. These LCCs also have the largest annual variation in LAI, which is represented differently in the different models, and this contributes to differences in the seasonal amplitude in total  $\text{O}_3$  deposition. In contrast, the differences in seasonal amplitude in total  $\text{O}_3$  dry deposition for water and grassland are likely due to the large areas covered by these LCCs as differences in the seasonal amplitude in  $\text{O}_3$  dry deposition velocities for these LCCs is small.

This analysis shows that the amplitude of the seasonal cycle in  $\text{O}_3$  dry deposition differs substantially across the models. This is particularly apparent for LCCs that are predom-

inant at northern mid to high latitudes (deciduous forests, coniferous forests, mixed forests, tundra, agricultural and cropland) and grasslands. The seasonal amplitude is expected to be large at northern mid and high latitudes where there is a well-defined seasonal cycle in LAI and meteorology. However, the range in seasonal amplitudes suggests that seasonality in vegetation (LAI, etc.) or meteorology is somewhat different within the various models, in agreement with our findings in Sect. 4.1.

Comparison of Figs. 4 and 5 shows that differences in the seasonal amplitude of  $\text{O}_3$  dry deposition to individual LCCs across the models remain small compared to the differences in total deposition. However, improved constraints on the seasonal amplitude in fluxes to seasonally dependent LCCs, e.g. through consideration of stomatal uptake as a function of environmental parameters, and more coherent representation of land cover and LAI across the models would contribute to a better representation of dry deposition.

## 5 Comparison with observed $\text{O}_3$ dry deposition fluxes

### 5.1 Long term measurements

Modelled  $\text{O}_3$  deposition fluxes are compared with measured fluxes at seven locations where at least one year of data is available. The measurement sites are summarized in Table 3. Monthly average  $\text{O}_3$  dry deposition fluxes were calculated at these sites and compared with model fluxes. Ozone fluxes were generally measured using the eddy covariance method or the aerodynamic flux gradient method (see references in Table 3). Uncertainty in  $\text{O}_3$  fluxes determined using these methods is around 12 % (Bauer et al., 2000; Muller et al., 2010). All seven sites are located in the Northern Hemisphere, and hence “summer”, “winter” and “growing season” in the following sections refer to NH timings for these periods.

The modelled and observed monthly  $\text{O}_3$  dry deposition fluxes are compared in Figs. 6 and 7. At each site the observed monthly fluxes were averaged across a number of years (the measurement period is indicated in Table 3) and the simulated monthly fluxes were averaged across the model ensemble.  $\text{O}_3$  dry deposition velocities and surface  $\text{O}_3$  concentrations were also compared at these sites. For each comparison, the seasonality and bias were assessed using the Pearson correlation coefficient and the line of best fit. The seasonality of the observed and modelled  $\text{O}_3$  dry deposition fluxes are shown in more detail in Fig. 8 where the average monthly fluxes are shown for each year of measurements and for each model. Measurements from Harvard Forest in 2005 were not available between June and August and were exceptionally low in May, September and November for that year.

At Ulborg, Hyttiala, Harvard Forest, the citrus orchard and Blodgett Forest the correlation coefficients for the com-



**Table 3.** O<sub>3</sub> dry deposition measurement sites.

Site name	Grid reference	Land cover	Sampling height/m	LAI	Sampling period	Reference
Long term sites						
Ulborg (Denmark)	56°17' N 8°25' E	Mixed coniferous forest	18, 36	8	Oct 1995–Dec 2000	Mikkelsen et al. (2004, 2000)
Castel Porziano (Italy)	41°44' N 12°24' E	Holm Oak forest	35	4.76	Jan 2013–Dec 2013	Fares et al. (2014)
Auchencorth Moss (Scotland)	55°47' N 3°14' W	Moorland	0.3–3.0	NA <sup>a</sup>	Jan 1995–Dec 1998	Fowler et al. (2001)
Hyytiälä (Finland)	61°51' N 24°17' E	Scots Pine forest	23	6–8	Jan 2002–Dec 2003	Rannik et al. (2012)
Harvard Forest (MA, USA)	42°32' N 72°11' W	Mixed deciduous forest	30	3.4	Jan 1992–Dec 2001	Munger et al. (1996)
Citrus orchard (CA, USA)	36°21' N 119°5' W	Citrus orchard	1.0–9.2	3.0	Oct 2009–Nov 2010	Fares et al. (2012)
Blodgett Forest (CA, USA)	38°53' N 120°37' W	Pine plantation	12.5	1.2–2.9	Jan 2001–Dec 2007	Fares et al. (2010)
Short term sites						
Danum Valley (Borneo)	4°58' N 117°51' E	Tropical forest	75	6	Apr, Jul 2008	Fowler et al. (2011)
Sabahmas (Borneo)	5°15' N 118°27' E	Oil palm	15	6	Apr 2008	Fowler et al. (2011)
South-western Amazon (Brazil)	3° S 60° W	Tropical forest	53	5.6	May 1999 Sep–Oct 1999	Rummel et al. (2007)
Central Amazon (Brazil)	10°5' N 61°55' W	Tropical forest	39		Apr–May 1987	Fan et al. (1990)
Grignon (France)	48°51' N 1°58' E	Maize crop	3.4, 6.4, 3.7	5.3–3.6	Apr 2008–Sep2008	Stella et al. (2011)
La Cape Sud (France)	44°24' N 0°38' E	Maize crop	3.4, 6.4, 3.7	5.1	Jul 2007–Oct 2007	Stella et al. (2011)
Lamasquere (France)	43°49' N 1°23' E	Maize crop	3.4, 6.4, 3.7	3.2	May 2008–Sep 2008	Stella et al. (2011)
Castel Porziano <sup>b</sup> (Italy)	41°43' N 12°23' E	Pseudo-steppe	8, 2	NA	Jun 1993, May 1994	Cieslik and Labatut (1997)
Burriana (Spain)	39°55' N 0°03' W	Citrus orchard	10	NA	16–29 Jul 1995 28 Apr–3 May 1996	Cieslik (2004)
Voghera (Italy)	45°01' N 9°00' E	Onion field	2.5	NA	May–Jul 2003	Gerosa et al. (2007)
Le Dezert (France)	44°05' N 0°43' E	Pine forest	37	NA	16–18 Apr 1997	Cieslik (2004)
Klippeneck (Germany)	48°10' N 8°45' E	Grass	2, 8	NA	10–22 Sep 1992	Cieslik (2004)
San Pietro Capofiume (Italy)	44°39' N 11°37' E	Beet crop	8	NA	15–22 Jun 1993	Cieslik (2004)
Viols en Levant (France)	43°41' N 3°47' E	Mediterranean shrub	37	NA	16–24 Jul 1998	Cieslik (2004)
Gilchriston Farm (Scotland)	56° N 3° E	Potato crop	2.2	NA	Jul	Coyle et al. (2009)

<sup>a</sup> NA: the data were not reported in the study. <sup>b</sup> The short term measurements made at Castel Porziano were part of a different campaign from the long term data set and were made at a different location.

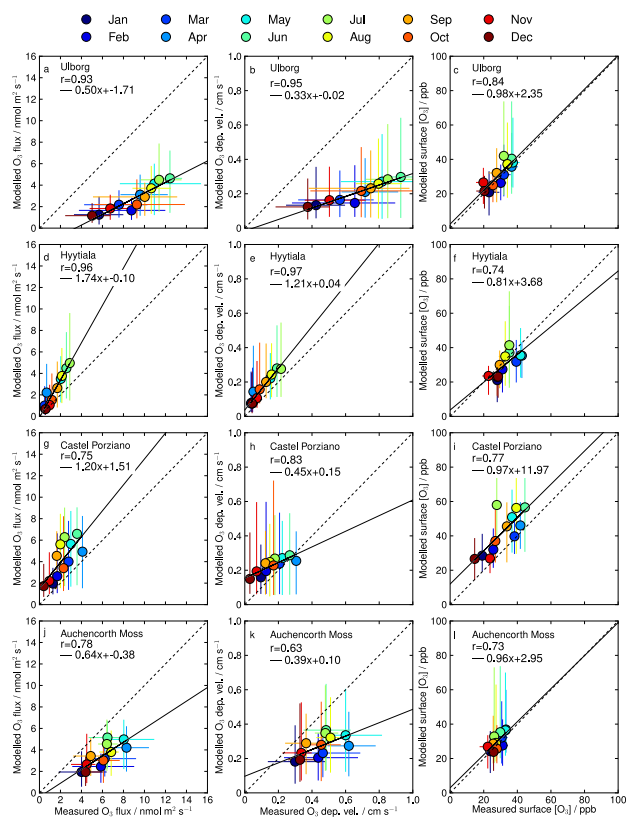


**Figure 6.** Comparison of observed and modelled monthly average  $\text{O}_3$  dry deposition fluxes,  $\text{O}_3$  dry deposition velocities and surface  $\text{O}_3$  at European measurement sites. Individual sites are shown by row for Ulborg (a–c), Hyytiälä (d–f), Castel Porziano (g–i) and Auchencorth Moss (j–l). Observed and modelled fluxes at each site are compared directly in the left hand column, deposition velocities are shown in the middle column, and surface  $\text{O}_3$  is compared in the right hand column. Vertical bars represent the range across the models and horizontal bars represent the interannual range in the observations, where available.

parison between the observed and modelled  $\text{O}_3$  dry deposition fluxes are greater than 0.85, indicating that the models are able to capture the seasonal cycle in  $\text{O}_3$  dry deposition well at these sites. The lower correlation coefficients at Castel Porziano and Auchencorth Moss reflect a difference in the timing of the peak fluxes in summertime. Observed fluxes were greatest in April and May, whereas the models simulated peak fluxes in June, as shown in Fig. 8.

$\text{O}_3$  dry deposition fluxes and surface  $\text{O}_3$  at Auchencorth Moss suggest that the early peak in  $\text{O}_3$  dry deposition is driven by relatively high surface  $\text{O}_3$  at this time. At Castel Porziano, surface  $\text{O}_3$  concentrations in April and May are lower than in summertime, suggesting that high dry deposition velocities drive the greater springtime fluxes at this site.

The slope of the best fit lines for the modelled and observed  $\text{O}_3$  dry deposition fluxes lie between 0.27 and 1.74 across the different measurement sites. Ozone dry deposition

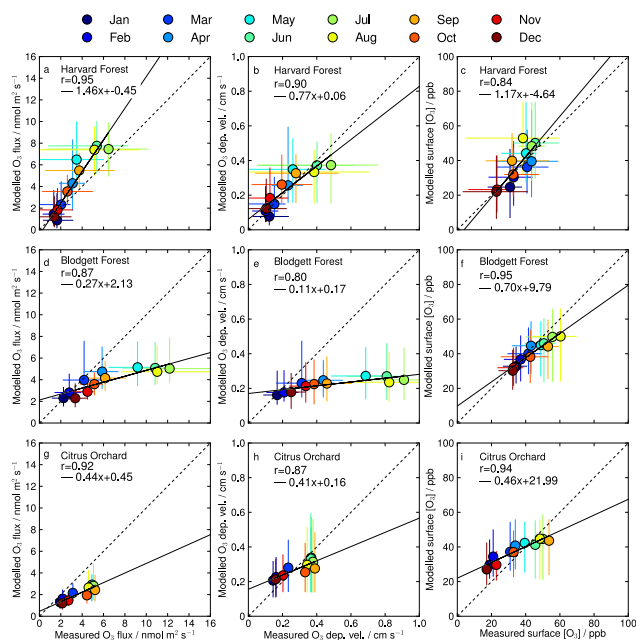


**Figure 7.** Comparison of observed and modelled monthly average  $\text{O}_3$  dry deposition fluxes,  $\text{O}_3$  dry deposition velocities and surface  $\text{O}_3$  at North American measurement sites. Individual sites are shown by row for Harvard Forest (a–c), Blodgett Forest (d–f) and Californian citrus orchard (g–i). Observed and modelled fluxes at each site are compared directly in the left hand column, deposition velocities are shown in the middle column, and surface  $\text{O}_3$  is compared in the right hand column. Vertical bars represent the range across the models and horizontal bars represent the interannual range in the observations, where available.

fluxes were underestimated at Ulborg, Auchencorth Moss and Blodgett Forest, and overestimated at Harvard Forest and Hyytiälä. The best agreement between the modelled and observed fluxes was at the citrus orchard site, where the models slightly overestimated  $\text{O}_3$  dry deposition throughout the year, although it should be noted that only a single year of data was available for this site. Although the number of sites is small, we do not find any clear systematic bias in  $\text{O}_3$  dry deposition fluxes over the sites as a whole.

We find a greater discrepancy between the modelled and measured  $\text{O}_3$  dry deposition fluxes in the growing season than in the winter months at all of the measurement sites except the citrus orchard. These biases do not appear to result from poor simulation of the seasonal cycle in the surface  $\text{O}_3$ , as this is generally captured well. Rather, it appears that the seasonal amplitude in  $\text{O}_3$  dry deposition fluxes is not represented well in the models. For example, at Blodgett Forest the observed fluxes during the growing season are 2–3 times greater than the modelled fluxes over the same period (Fig. 8g). In contrast, at Hyytiälä, the modelled growing season fluxes are approximately twice as large as the observed fluxes (Fig. 8d).

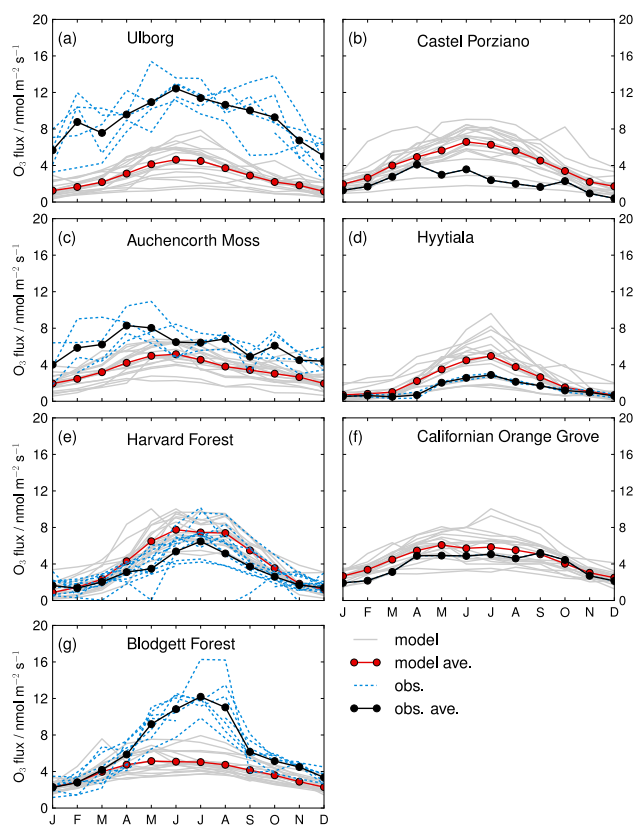


**Figure 8.** Measured and modelled monthly average  $O_3$  dry deposition fluxes at Ulborg (a), Castel Porziano (b), Auchencorth Moss (c), Hyytiala (d), Harvard Forest (e), Californian citrus orchard (f), and Blodgett Forest (g). Grey lines show results from individual models and blue lines show observations for different years.

Surface  $O_3$  and its seasonal cycle are generally captured well by the models at all of the measurement sites. The correlation coefficients lie between 0.73 and 0.94 and the slopes range from 0.46 to 0.97. Consequently, the modelled dry deposition velocities do not match the measurement data better than the dry deposition fluxes, although there is less seasonal variation in the dry deposition velocities as the observed seasonal cycle in surface  $O_3$  is captured well. This indicates that biases in modelled  $O_3$  dry deposition fluxes are due to the representation of dry deposition velocities rather than biases in surface  $O_3$ .

## 5.2 Partitioned modelled $O_3$ dry deposition fluxes

Comparing point observations with modelled  $O_3$  dry deposition fluxes presents a number of challenges. Measurement sites may not be representative of the model grid cell, and the grid cell may not provide an accurate representation of the land cover at the site. Figure 9 shows a comparison between observed fluxes and the modelled fluxes partitioned between the various LCCs located in the grid cell in which the mea-

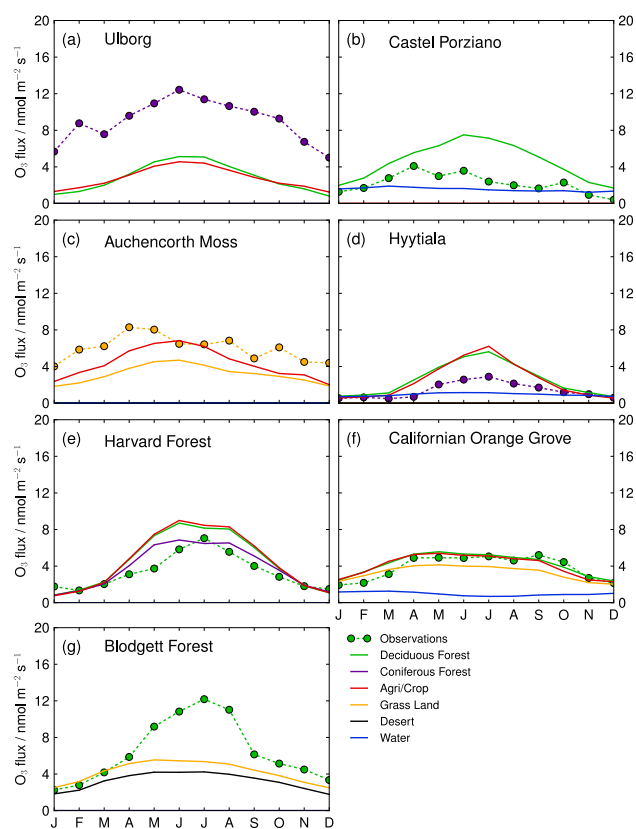


**Figure 9.** Observed monthly average  $O_3$  dry deposition fluxes at measurement sites (dashed lines) and repartitioned model fluxes for each land cover class (solid lines). Colours indicate the LCC at the site and in the model grid cell containing the site.

surement site was located. LCC coverage for the model grid cells was obtained from the OW11 land cover data set which described fractional land cover.

It is clear that in some cases the LCC at the measurement site is not represented in the corresponding model grid cell. The Ulborg and Hyytiala measurement sites are situated in coniferous forests, but the OW11 data set does not include coniferous forest in the corresponding grid cells. The partitioned fluxes for deciduous forest and agricultural cropland at Ulborg, and for deciduous forest, agricultural cropland and water at Hyytiala are not found to be in better agreement with the observed  $O_3$  dry deposition fluxes than the total modelled flux. Similarly, at Blodgett Forest in California, a deciduous forest site, the land cover classes are desert and grassland, and this partly explains the model underestimation of fluxes here.

At Auchencorth Moss, Harvard Forest and the citrus orchard there is better agreement in LCCs between the OW11 data set and the measurement site. At these sites fluxes partitioned to more relevant LCCs are generally in better agreement with the observed fluxes. At the Californian citrus orchard the fluxes to cropland and deciduous forest fit the ob-

served fluxes very well. At Auchencorth Moss, the flux partitioned to crop land is in slightly better agreement with the observations than that due to grassland. At Harvard Forest, the flux partitioned to deciduous forest is higher than that observed, and the flux to coniferous forest is somewhat closer.

We have demonstrated that selecting an appropriate land cover class can lead to improved agreement between modelled and observed  $O_3$  dry deposition fluxes, although this is not always the case. This analysis highlights the difficulties in comparing modelled fluxes with observations, particularly where an appropriate land cover class is unavailable. However, our findings suggest that future comparison of modelled and observed fluxes should be based on model-diagnosed fluxes to the most relevant land cover class within a grid cell using the native LCC scheme in the model, not merely total fluxes at the correct geographical location.

### 5.3 CASTNET sites

Modelled  $O_3$  dry deposition fluxes, dry deposition velocity and surface  $O_3$  were compared with average monthly values at 96 CASTNET sites grouped according to land cover class, see Fig. 10. The Pearson correlation coefficient and the slope of the line of best fit value are shown for the individual sites in the Supplementary information. The seasonal cycle in  $O_3$  dry deposition flux is generally well represented by the models at the forest, grassland and crop sites with  $r^2$  values generally greater than 0.8. However, at these sites the models tend to overestimate  $O_3$  dry deposition fluxes by about 30%. Conversely at the shrub and desert sites the models often underestimate the  $O_3$  dry deposition fluxes and do not capture any seasonal variation well. Several, although not all, of these sites were situated in terrain classified as “complex” or “mountain top”.

Comparison between the modelled and CASTNET  $O_3$  dry deposition velocities and surface  $O_3$  show that while surface  $O_3$  is generally well represented in the models (as also seen in Fiore et al., 2009), dry deposition velocities are represented less well. This suggests that the bias in modelled  $O_3$  dry deposition fluxes is driven by bias in the modelled  $O_3$  dry deposition velocity rather than bias in the modelled surface  $O_3$ . In particular, the seasonal cycle is not captured well, with modelled deposition velocities too high in the spring and autumn months, suggesting that the increase in  $O_3$  dry deposition velocity from winter to summer occurs too soon.

It is not clear from this comparison alone what is driving the disparity between the modelled and CASTNET  $O_3$  dry deposition velocities. However, the differences are most pronounced for the forest and cropland LCCs. Changes in LAI during spring and summer are expected to be greatest for these LCCs, suggesting that this parameter is not well represented in these global scale models. Diagnosis of LAI in future model studies would allow the influence of this variable to be determined more clearly.

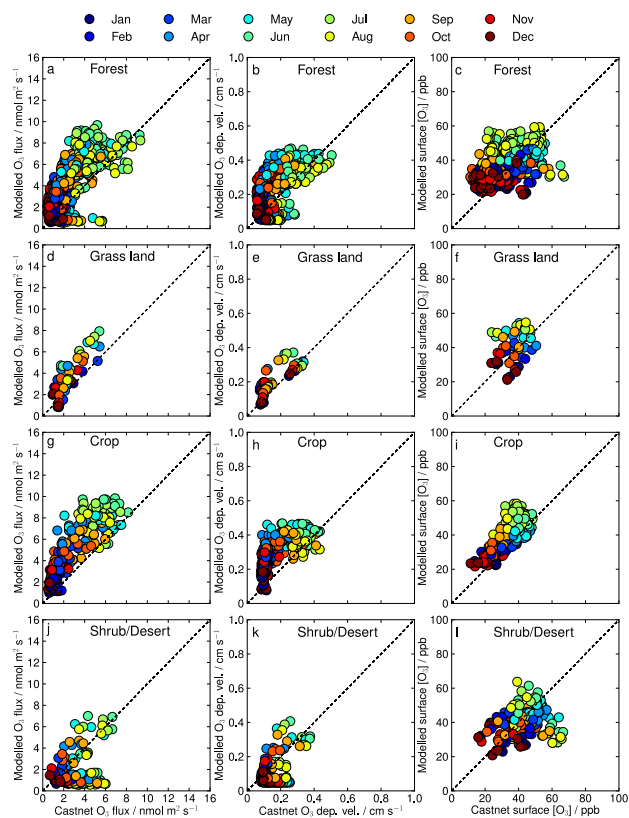


**Figure 10.** Comparison of CASTNET and modelled monthly average  $O_3$  dry deposition fluxes,  $O_3$  dry deposition velocities and surface  $O_3$  at CASTNET measurement sites. The CASTNET sites are grouped by land cover class which are shown by row for forest sites (a–c), grassland sites (d–f), crop sites (g–i) and shrub/desert sites (j–l). CASTNET and modelled fluxes at each site are compared in the left hand column, deposition velocities are shown in the middle column, and surface  $O_3$  is compared in the right hand column.

### 5.4 Short term measurements

Modelled  $O_3$  dry deposition fluxes were compared with observations at a number of sites where short term flux measurements are available; see Table 3. Figure 11 shows that agreement between the observed and modelled  $O_3$  dry deposition fluxes are variable at these sites. At crop sites, the models generally overestimated fluxes to the maize crops, but underestimated fluxes at other crop locations.  $O_3$  dry deposition fluxes are overestimated at the coniferous forest, but underestimated at the other shrub locations.

The modelled and measured  $O_3$  dry deposition fluxes agreed well at the tropical forest and oil palm sites in Malaysian Borneo, but less well at the Amazonian tropical forest sites. There was also less variation in  $O_3$  dry deposition fluxes across the models at the Malaysian Borneo sites than at the Amazonian sites, possibly due to the large fraction of ocean in the Malaysian Borneo grid cell. Variation in the modelled  $O_3$  dry deposition fluxes at the Amazonian

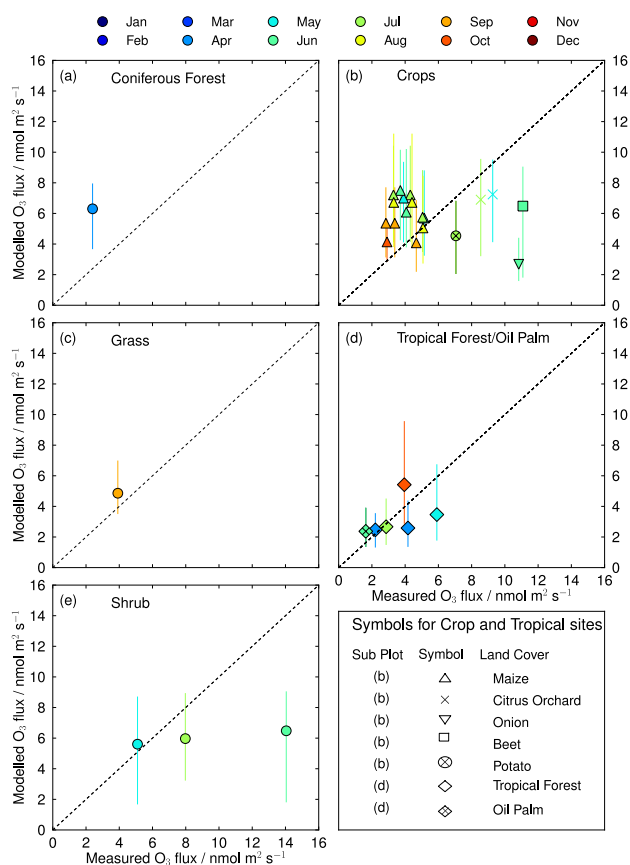


**Figure 11.** Measured and modelled monthly average  $O_3$  dry deposition fluxes at short term measurement sites. Colours indicate the average flux for the relevant month and shapes indicate the measurement site.

sites is similar to that in the tropical forests shown in Fig. 3. The temporally and spatially limited scale of the measurement data makes it difficult to draw conclusions about model performance at tropical forest sites, but there does not appear to be systematic bias for this LCC.

The short term crop, coniferous forest, grass and shrub sites were all located in Europe and the models did not capture the range in  $O_3$  dry deposition fluxes that were observed at these sites. However, the regional average observed flux over these sites ( $7.9\ nmol\ m^{-2}\ s^{-1}$ ) lies close to the range of the modelled fluxes ( $5.8 \pm 2.1\ nmol\ m^{-2}\ s^{-1}$ ), suggesting that there is no clear systematic bias in the modelled fluxes over this region.

It is likely that models are unable to capture the spatial variability in  $O_3$  dry deposition at the European sites given the coarse grid resolution used here. The measurement sites span a range of heterogeneous land cover types, including natural and semi-natural vegetation as well as agricultural and urban areas, within a relatively small geographical region. This heterogeneity is not captured in the OW11 land cover data set, which assigns a similar combination of

coniferous forest, deciduous forest, grassland and agricultural/crop land to grid cells in the western European region. There will be a similar lack of spatial resolution in the native land cover schemes in the models.

The short timescales over which these measurements were made renders it difficult to assess how well the models capture the seasonality at these sites. Measurements at Castel Porziano (Mediterranean pseudo-steppe) and Burriana (citrus orchard) covered two different months in different years. At Burriana the difference in  $O_3$  dry deposition fluxes between May and July is small, in agreement with observations in the Californian citrus orchard. At the Castel Porziano site there is a much greater difference between  $O_3$  dry deposition fluxes observed in May and June in the different years, probably representing meteorological differences over the relatively short observation periods.

The comparison between these observations and the global scale models highlights the difficulty in comparing models with observations, especially in regions with very heterogeneous land cover such as western Europe. This was also noted in the evaluation of the EMEP (Tuovinen et al., 2004, 2009) and AURAMS (Zhang et al., 2002) models. While a finer resolution global or regional scale model may be able to capture the spatial variability in  $O_3$  dry deposition observed here, better diagnosis of land cover specific fluxes would be valuable to identify the key weaknesses in current model deposition schemes. Previous evaluations of the EMEP and AURAMS models suggest that soil moisture deficit and parameterization of non-stomatal fluxes represent key uncertainties in the dry deposition schemes implemented in regional scale models and are likely to contribute to the discrepancies between modelled and measured fluxes observed in this study. In addition, near-surface and in-canopy chemistry of  $O_3$  (Chang et al., 2004; Wolfe et al., 2011) is not accounted for in the global scale models used in this study. These processes occur at small physical scales, but may contribute to differences between modelled and measured fluxes. Our comparison further highlights the need for spatially representative flux measurements over extended periods (ideally seasonal to annual periods) that are not greatly affected by the short term variability in meteorology or vegetation properties.

## 6 Conclusions

This study provides the first analysis of  $O_3$  dry deposition fluxes in global scale chemistry climate models. We identify regions where  $O_3$  dry deposition differs substantially across an ensemble of 15 global models and show how land cover drives these differences. We also compare modelled  $O_3$  dry deposition fluxes to observations at a range of measurement sites.

An initial assessment of  $O_3$  dry deposition across latitudes shows that it is most variable between southern and north-



ern mid-latitudes, and the extent of the variation across the models is dependent on the season. The greatest differences in total O<sub>3</sub> dry deposition across the models occur where deposition velocities and surface O<sub>3</sub> concentrations are highest. The particularly large differences in deposition at tropical latitudes are driven by a small number of models which simulate comparatively low surface O<sub>3</sub> in this region. These results indicate the need for better constraints on O<sub>3</sub> dry deposition during the growing season and at tropical latitudes.

To investigate the causes of the differences in dry deposition across the models, fluxes were partitioned to land cover class. We find that differences in O<sub>3</sub> dry deposition flux to oceans, driven by small absolute differences in dry deposition velocity, are the largest contributor to differences in the global O<sub>3</sub> deposition flux. Over continental regions, deposition to grasslands showed the greatest difference between models. Again, this was driven by relatively small absolute differences in deposition velocity integrated over the 8–9 % of the global surface area covered by grassland. Modelled O<sub>3</sub> dry deposition fluxes differed most over tropical forests, suggesting large differences in deposition velocity and the absence of this land cover class in some models. The magnitude of the deposition to oceans means that it is important for the global ozone budget that this term is constrained better. However, deposition to terrestrial ecosystems has important implications for many other components of the Earth system including carbon sequestration, hydrology and atmospheric composition.

This comparison of O<sub>3</sub> dry deposition partitioned to LCC demonstrates that differences in total O<sub>3</sub> dry deposition across the models could be greatly reduced by improved constraints on deposition velocities, particularly to oceans, grasslands and tropical forests. The importance of well-constrained fluxes to oceans was noted by Ganzeveld et al. (2009), who found that small differences in O<sub>3</sub> dry deposition flux could drive large differences in tropospheric O<sub>3</sub>. Differences in O<sub>3</sub> deposition to grasslands or tropical forests will have a much smaller effect on the global tropospheric O<sub>3</sub> burden, but may significantly impact local atmospheric composition.

We highlight the degree of variation in ozone dry deposition that results from differences in the land cover classification used in the different global scale models. Some models use very limited land cover schemes with as few as five LCCs, and this may be a particular problem for simpler Earth System Models where vegetation processes are explicitly simulated online. This results in some LCCs, e.g. tropical forest, being omitted altogether. Further, deposition flux measurements are available from a relatively limited range of land cover classes, so differences in mapping these to the native LCC scheme leads to differing global coverage and deposition in different models. This may lead to substantial differences in local surface O<sub>3</sub> even though the global O<sub>3</sub> burden is not greatly affected. Tropical forests are important regions for atmospheric processing, for example, and obser-

vations have shown that O<sub>3</sub> dry deposition is relatively fast in these locations. Application of a generic deciduous forest or forest to this land cover therefore results in underestimation of O<sub>3</sub> deposition fluxes and a systematic bias in the chemical environment here.

We do not have sufficient data from the HTAP model study to assess the impact of other biases which are likely to drive model differences in O<sub>3</sub> dry deposition. Biases in the diurnal cycle of deposition fluxes and partitioning between stomatal and non-stomatal fluxes are likely to be cumulative across large areas and may have a significant effect on global annual O<sub>3</sub> dry deposition. While global scale model intercomparison projects have not previously reported O<sub>3</sub> dry deposition at this level of detail, we recommend that future model comparisons request these additional flux diagnostics to allow deposition processes to be tested more thoroughly.

In this study we make the first assessment of O<sub>3</sub> dry deposition fluxes in global models against observations. The models generally simulate the seasonal variations in O<sub>3</sub> dry deposition fluxes well. While our comparison of modelled O<sub>3</sub> deposition fluxes with direct flux observations did not show a systematic bias, comparison with fluxes derived from CASTNET observations suggests that the models overestimate O<sub>3</sub> dry deposition fluxes over North America. In general, we find that the discrepancy between modelled and observed O<sub>3</sub> dry deposition fluxes is driven by the modelled O<sub>3</sub> dry deposition velocity rather than by surface O<sub>3</sub>, but this is not the case at all sites.

This comparison between the models and observations provides an initial set of metrics that can be used as a simple indicator of model performance. More critical testing of model performance will require more detailed diagnostics of O<sub>3</sub> dry deposition, including fluxes partitioned by land cover class, stomatal and non-stomatal fluxes, and fluxes at higher temporal resolution to explore the diurnal behaviour. It will also be important to have long term flux measurements, over at least a full seasonal cycle, from sites with land cover classes that are broadly representative of a wider region. Characterization of deposition velocities over a wide range of land cover classes would be particularly valuable for refining the variables used in current model resistance schemes, including over the ocean, where differences between models are large. These should allow us to place better constraints on this important term in the global O<sub>3</sub> budget.

**The Supplement related to this article is available online at doi:10.5194/acp-15-6419-2015-supplement.**

*Acknowledgements.* This work was supported by the Natural Environment Research Council [grant number NE/K001272/1] as part of the Atmospheric Chemistry in the Earth System (ACITES) network. We acknowledge the modelling groups who contributed

to the HTAP model intercomparison project and provided the model results we have used in this study. We are also grateful to the following for generously allowing their valuable measurement data to be used here: Nuria Altimir (University of Helsinki, Finland), Stanislaw Cieslik (formerly at the Joint Research Centre), Mhairi Coyle (Centre for Ecology and Hydrology, Edinburgh), Silvano Fares (Agricultural Research Council, Italy), Allen Goldstein (University of California at Berkeley, USA), Teis Mikkelsen (Technical University of Denmark, Denmark), Bill Munger (Harvard University, USA) and the following from the National Institute for Agronomic Research and CESBIO, France: P. Stella, E. Personne, B. Loubet, E. Lamaud, E. Ceschia, P. Beziat, J. M. Bonnefond, M. Irvine, P. Keravec, N. Mascher, P. Cellier, E. Larmanou, O. Fanucci, B. Durand, C. Decuq, M. Burban, P. Duprix, S. Debesa, D. Garrigou, H. Gibrin, N. Ferroni, B. Marciel and A. Kruszwski.

Edited by: L. Ganzeveld

## References

- Ainsworth, E. A., Yendrek, C. R., Sitch, S., Collins, W. J., and Emberson, L. D.: The Effects of Tropospheric Ozone on Net Primary Productivity and Implications for Climate Change, *Annu. Rev. Plant Biol.*, 63, 637–661, doi:10.1146/annurev-arplant-042110-103829, 2012.
- Anenberg, S. C., Horowitz, L. W., Tong, D. Q., and West, J. J.: An Estimate of the Global Burden of Anthropogenic Ozone and Fine Particulate Matter on Premature Human Mortality Using Atmospheric Modeling, *Environ. Health Persp.*, 118, 1189–1195, doi:10.1289/ehp.0901220, 2010.
- Arnth, A., Harrison, S. P., Zaehle, S., Tsigaridis, K., Menon, S., Bartlein, P. J., Feichter, J., Korhola, A., Kulmala, M., O'Donnell, D., Schurgers, G., Sorvari, S., and Vesala, T.: Terrestrial biogeochemical feedbacks in the climate system, *Nat. Geosci.*, 3, 525–532, doi:10.1038/ngeo905, 2010.
- Ashmore, M. R.: Assessing the future global impacts of ozone on vegetation, *Plant Cell Environ.*, 28, 949–964, doi:10.1111/j.1365-3040.2005.01341.x, 2005.
- Atkinson, R.: Atmospheric chemistry of VOCs and NO<sub>x</sub>, *Atmos. Environ.*, 34, 2063–2101, doi:10.1016/S1352-2310(99)00460-4, 2000.
- Avnery, S., Mauzerall, D. L., Liu, J., and Horowitz, L. W.: Global crop yield reductions due to surface ozone exposure: 1. Year 2000 crop production losses and economic damage, *Atmos. Environ.*, 45, 2284–2296, doi:10.1016/j.atmosenv.2010.11.045, 2011a.
- Avnery, S., Mauzerall, D. L., Liu, J., and Horowitz, L. W.: Global crop yield reductions due to surface ozone exposure: 2. Year 2030 potential crop production losses and economic damage under two scenarios of O<sub>3</sub> pollution, *Atmos. Environ.*, 45, 2297–2309, doi:10.1016/j.atmosenv.2011.01.002, 2011b.
- Bauer, M. R., Hultman, N. E., Panek, J. A., and Goldstein, A. H.: Ozone deposition to a ponderosa pine plantation in the Sierra Nevada Mountains (CA): A comparison of two different climatic years, *J. Geophys. Res.-Atmos.*, 105, 22123–22136, doi:10.1029/2000JD900168, 2000.
- Bey, I., Jacob, D. J., Yantosca, R. M., Logan, J. A., Field, B. D., Fiore, A. M., Li, Q. B., Liu, H. G. Y., Mickley, L. J., and Schultz, M. G.: Global modeling of tropospheric chemistry with assimilated meteorology: Model description and evaluation, *J. Geophys. Res.-Atmos.*, 106, 23073–23095, doi:10.1029/2001JD000807, 2001.
- Buker, P., Emberson, L. D., Ashmore, M. R., Cambridge, H. M., Jacobs, C. M. J., Massman, W. J., Muller, J., Nikolov, N., Novak, K., Oksanen, E., Schaub, M., and de la Torre, D.: Comparison of different stomatal conductance algorithms for ozone flux modelling, *Environ. Pollut.*, 146, 726–735, doi:10.1016/j.envpol.2006.04.007, 2007.
- Chang, W. N., Heikes, B. G., and Lee, M. H.: Ozone deposition to the sea surface: chemical enhancement and wind speed dependence, *Atmos. Environ.*, 38, 1053–1059, doi:10.1016/j.atmosenv.2003.10.050, 2004.
- Cieslik, S. and Labatut, A.: Ozone surface fluxes and stomatal activity, *Proceedings of Eurotrac Symposium '96 – Transport and Transformation of Pollutants In the Troposphere, Vol. 2: Emissions, Deposition, Laboratory Work and Instrumentation*, 177–184, 1997.
- Cieslik, S. A.: Ozone uptake by various surface types: a comparison between dose and exposure, *Atmos. Environ.*, 38, 2409–2420, doi:10.1016/j.atmosenv.2003.10.063, 2004.
- Clarke, J. F., Edgerton, E. S., and Martin, B. E.: Dry deposition calculations for the clean air status and trends network, *Atmos. Environ.*, 31, 3667–3678, doi:10.1016/S1352-2310(97)00141-6, 1997.
- Collins, W. J., Stevenson, D. S., Johnson, C. E., and Derwent, R. G.: Tropospheric Ozone in a Global-Scale Three-Dimensional Lagrangian Model and Its Response to NO<sub>x</sub> Emission Controls, *J. Atmos. Chem.*, 26, 223–274, doi:10.1023/A:1005836531979, 1997.
- Collins, W. J., Derwent, R. G., Garnier, B., Johnson, C. E., Sanderson, M. G., and Stevenson, D. S.: Effect of stratosphere-troposphere exchange on the future tropospheric ozone trend, *J. Geophys. Res.-Atmos.*, 108, 8528, doi:10.1029/2002JD002617, 2003.
- Coyle, M., Nemitz, E., Storeton-West, R., Fowler, D., and Cape, J. N.: Measurements of ozone deposition to a potato canopy, *Agr. Forest Meteorol.*, 149, 655–666, doi:10.1016/j.agrformet.2008.10.020, 2009.
- Crutzen, P. J.: Photochemical Reactions Initiated By and Influencing Ozone In Unpolluted Tropospheric Air, *Tellus*, 26, 47–57, 1974.
- De Fries, R. S. and Townshend, J. R. G.: Ndvi-derived Land-cover Classifications At A Global-scale, *Int. J. Remote Sens.*, 15, 3567–3586, 1994.
- Dentener, F., Drevet, J., Lamarque, J. F., Bey, I., Eickhout, B., Fiore, A. M., Hauglustaine, D., Horowitz, L. W., Krol, M., Kulshrestha, U. C., Lawrence, M., Galy-Lacaux, C., Rast, S., Shindell, D., Stevenson, D., Van Noije, T., Atherton, C., Bell, N., Bergman, D., Butler, T., Cofala, J., Collins, B., Doherty, R., Ellingsen, K., Galloway, J., Gauss, M., Montanaro, V., Mueller, J. F., Pitari, G., Rodriguez, J., Sanderson, M., Solmon, F., Strahan, S., Schultz, M., Sudo, K., Szopa, S., and Wild, O.: Nitrogen and sulfur deposition on regional and global scales: A multimodel evaluation, *Global Biogeochem. Cy.*, 20, GB4003, doi:10.1029/2005GB002672, 2006.
- Emberson, L. D., Ashmore, M. R., Cambridge, H. M., Simpson, D., and Tuovinen, J. P.: Modelling stomatal ozone flux across

- Europe, *Environ. Pollut.*, 109, 403–413, doi:10.1016/S0269-7491(00)00043-9, 2000a.
- Emberson, L. D., Wieser, G., and Ashmore, M. R.: Modelling of stomatal conductance and ozone flux of Norway spruce: comparison with field data, *Environ. Pollut.*, 109, 393–402, doi:10.1016/S0269-7491(00)00042-7, 2000b.
- Emberson, L. D., Ashmore, M. R., Simpson, D., Tuovinen, J. P., and Cambridge, H. M.: Modelling and mapping ozone deposition in Europe, *Water Air Soil Poll.*, 130, 577–582, doi:10.1023/A:1013851116524, 2001.
- Emberson, L. D., Kitwiroon, N., Beevers, S., Büker, P., and Cinderby, S.: Scorched Earth: how will changes in the strength of the vegetation sink to ozone deposition affect human health and ecosystems?, *Atmos. Chem. Phys.*, 13, 6741–6755, doi:10.5194/acp-13-6741-2013, 2013.
- Fan, S. M., Wofsy, S. C., Bakwin, P. S., Jacob, D. J., and Fitzjarrald, D. R.: Atmosphere-biosphere Exchange of CO<sub>2</sub> and O<sub>3</sub> In the Central-amazon-forest, *J. Geophys. Res.-Atmos.*, 95, 16851–16864, doi:10.1029/JD095iD10p16851, 1990.
- Fares, S., Park, J.-H., Ormeno, E., Gentner, D. R., McKay, M., Loreto, F., Karlik, J., and Goldstein, A. H.: Ozone uptake by citrus trees exposed to a range of ozone concentrations, *Atmos. Environ.*, 44, 3404–3412, doi:10.1016/j.atmosenv.2010.06.010, 2010.
- Fares, S., Weber, R., Park, J.-H., Gentner, D., Karlik, J., and Goldstein, A. H.: Ozone deposition to an orange orchard: Partitioning between stomatal and non-stomatal sinks, *Environ. Pollut.*, 169, 258–266, doi:10.1016/j.envpol.2012.01.030, 2012.
- Fares, S., Savi, F., Muller, J., Matteucci, G., and Paoletti, E.: Simultaneous measurements of above and below canopy ozone fluxes help partitioning ozone deposition between its various sinks in a Mediterranean Oak Forest, *Agr. Forest Meteorol.*, 198–199, 181–191, 2014.
- Finkelstein, P. L., Ellestad, T. G., Clarke, J. F., Meyers, T. P., Schwede, D. B., Hebert, E. O., and Neal, J. A.: Ozone and sulfur dioxide dry deposition to forests: Observations and model evaluation, *J. Geophys. Res.-Atmos.*, 105, 15365–15377, doi:10.1029/2000JD900185, 2000.
- Fiore, A. M., Dentener, F. J., Wild, O., Cuvelier, C., Schultz, M. G., Hess, P., Textor, C., Schulz, M., Doherty, R. M., Horowitz, L. W., MacKenzie, I. A., Sanderson, M. G., Shindell, D. T., Stevenson, D. S., Szopa, S., Van Dingenen, R., Zeng, G., Atherton, C., Bergmann, D., Bey, I., Carmichael, G., Collins, W. J., Duncan, B. N., Faluvegi, G., Folberth, G., Gauss, M., Gong, S., Hauglustaine, D., Holloway, T., Isaksen, I. S. A., Jacob, D. J., Jonson, J. E., Kaminski, J. W., Keating, T. J., Lupu, A., Marmor, E., Montanaro, V., Park, R. J., Pitari, G., Pringle, K. J., Pyle, J. A., Schroeder, S., Vivanco, M. G., Wind, P., Wojcik, G., Wu, S., and Zuber, A.: Multimodel estimates of intercontinental source-receptor relationships for ozone pollution, *J. Geophys. Res.-Atmos.*, 114, D04301, doi:10.1029/2008JD010816, 2009.
- Fowler, D., Flechard, C., Cape, J. N., Storeton-West, R. L., and Coyle, M.: Measurements of ozone deposition to vegetation quantifying the flux, the stomatal and non-stomatal components, *Water Air Soil Poll.*, 130, 63–74, doi:10.1023/A:1012243317471, 2001.
- Fowler, D., Pilegaard, K., Sutton, M. A., Ambus, P., Raivonen, M., Duyzer, J., Simpson, D., Fagerli, H., Fuzzi, S., Schjoerring, J. K., Granier, C., Neftel, A., Isaksen, I. S. A., Laj, P., Maione, M., Monks, P. S., Burkhardt, J., Daemmgen, U., Neiryneck, J., Perronne, E., Wichink-Kruit, R., Butterbach-Bahl, K., Flechard, C., Tuovinen, J. P., Coyle, M., Gerosa, G., Loubet, B., Altimir, N., Gruenhage, L., Ammann, C., Cieslik, S., Paoletti, E., Mikkelsen, T. N., Ro-Poulsen, H., Cellier, P., Cape, J. N., Horvath, L., Loreto, F., Niinemets, U., Palmer, P. I., Rinne, J., Misztal, P., Nemitz, E., Nilsson, D., Pryor, S., Gallagher, M. W., Vesala, T., Skiba, U., Brüggemann, N., Zechmeister-Boltenstern, S., Williams, J., O'Dowd, C., Facchini, M. C., de Leeuw, G., Flossman, A., Chaumerliac, N., and Erisman, J. W.: Atmospheric composition change: Ecosystems-Atmosphere interactions, *Atmos. Environ.*, 43, 5193–5267, doi:10.1016/j.atmosenv.2009.07.068, 2009.
- Fowler, D., Nemitz, E., Misztal, P., Di Marco, C., Skiba, U., Ryder, J., Helfter, C., Cape, J. N., Owen, S., Dorsey, J., Gallagher, M. W., Coyle, M., Phillips, G., Davison, B., Langford, B., MacKenzie, R., Muller, J., Siong, J., Dari-Salisburgo, C., Di Carlo, P., Aruffo, E., Giammaria, F., Pyle, J. A., and Hewitt, C. N.: Effects of land use on surface-atmosphere exchanges of trace gases and energy in Borneo: comparing fluxes over oil palm plantations and a rainforest, *Philos. T. Roy. Soc. B*, 366, 3196–3209, doi:10.1098/rstb.2011.0055, 2011.
- Fuhrer, J.: Ozone risk for crops and pastures in present and future climates, *Naturwissenschaften*, 96, 173–194, doi:10.1007/s00114-008-0468-7, 2009.
- Ganzeveld, L. and Lelieveld, J.: Dry Deposition Parameterization In A Chemistry General-circulation Model and Its Influence On the Distribution of Reactive Trace Gases, *J. Geophys. Res.-Atmos.*, 100, 20999–21012, doi:10.1029/95JD02266, 1995.
- Ganzeveld, L., Helmig, D., Fairall, C. W., Hare, J., and Pozzer, A.: Atmosphere-ocean ozone exchange: A global modeling study of biogeochemical, atmospheric, and waterside turbulence dependencies, *Global Biogeochem. Cy.*, 23, GB4021, doi:10.1029/2008GB003301, 2009.
- Ganzeveld, L., Bouwman, L., Stehfest, E., van Vuuren, D. P., Eickhout, B., and Lelieveld, J.: Impact of future land use and land cover changes on atmospheric chemistry-climate interactions, *J. Geophys. Res.-Atmos.*, 115, D23301, doi:10.1029/2010JD014041, 2010.
- Gerosa, G., Derghi, F., and Cieslik, S.: Comparison of different algorithms for stomatal ozone flux determination from micrometeorological measurements, *Water Air Soil Poll.*, 179, 309–321, doi:10.1007/s11270-006-9234-7, 2007.
- Giannakopoulos, C., Chipperfield, T. P., Law, K. S., and Pyle, J. A.: Validation and intercomparison of wet and dry deposition schemes using Pb-210 in a global three-dimensional off-line chemical transport model, *J. Geophys. Res.-Atmos.*, 104, 23761–23784, doi:10.1029/1999JD900392, 1999.
- Hardacre, C. J., Palmer, P. I., Baumanns, K., Rounsevell, M., and Murray-Rust, D.: Probabilistic estimation of future emissions of isoprene and surface oxidant chemistry associated with land-use change in response to growing food needs, *Atmos. Chem. Phys.*, 13, 5451–5472, doi:10.5194/acp-13-5451-2013, 2013.
- Hauglustaine, D. A., Hourdin, F., Jourdain, L., Filiberti, M. A., Walters, S., Lamarque, J. F., and Holland, E. A.: Interactive chemistry in the Laboratoire de Meteorologie Dynamique general circulation model: Description and background tropospheric chemistry evaluation, *J. Geophys. Res.-Atmos.*, 109, D04314, doi:10.1029/2003JD003957, 2004.

- Helmig, D., Lang, E., Bariteau, L., Boylan, P., Fairall, C., Ganzeveld, L., Hare, J., Hueber, J., and Pallandt, M.: Atmosphere-ocean ozone fluxes during the TexAQS 2006, STRATUS 2006, GOMECC 2007, GasEX 2008 and AMMA 2008 cruises, *J. Geophys. Res.*, 117, D015955, doi:10.1029/2011JD015955, 2012.
- Hollaway, M. J.: Modelling Interactions Between Vegetation and Tropospheric Ozone, PhD thesis, University of Leeds, 2012.
- Horowitz, L. W., Walters, S., Mauzerall, D. L., Emmons, L. K., Rasch, P. J., Granier, C., Tie, X., Lamarque, J.-F., Schultz, M. G., Tyndall, G. S., Orlando, J. J., and Brasseur, G. P.: A global simulation of tropospheric ozone and related tracers: Description and evaluation of MOZART, version 2, *J. Geophys. Res.*, 108, 4784–4813, doi:10.1029/2002JD002853, 2003.
- Huijnen, V., Williams, J., van Weele, M., van Noije, T., Krol, M., Dentener, F., Segers, A., Houweling, S., Peters, W., de Laat, J., Boersma, F., Bergamaschi, P., van Velthoven, P., Le Sager, P., Eskes, H., Alkemade, F., Scheele, R., Nédélec, P., and Pätz, H.-W.: The global chemistry transport model TM5: description and evaluation of the tropospheric chemistry version 3.0, *Geosci. Model Dev.*, 3, 445–473, doi:10.5194/gmd-3-445-2010, 2010.
- Kaminski, J. W., Neary, L., Struzewska, J., McConnell, J. C., Lupu, A., Jarosz, J., Toyota, K., Gong, S. L., Côté, J., Liu, X., Chance, K., and Richter, A.: GEM-AQ, an on-line global multiscale chemical weather modelling system: model description and evaluation of gas phase chemistry processes, *Atmos. Chem. Phys.*, 8, 3255–3281, doi:10.5194/acp-8-3255-2008, 2008.
- Lamarque, J.-F., Emmons, L. K., Hess, P. G., Kinnison, D. E., Tilmes, S., Vitt, F., Heald, C. L., Holland, E. A., Lauritzen, P. H., Neu, J., Orlando, J. J., Rasch, P. J., and Tyndall, G. K.: CAM-chem: description and evaluation of interactive atmospheric chemistry in the Community Earth System Model, *Geosci. Model Dev.*, 5, 369–411, doi:10.5194/gmd-5-369-2012, 2012.
- Lelieveld, J. and Dentener, F. J.: What controls tropospheric ozone?, *J. Geophys. Res.*, 105, 3531–3551, doi:10.1029/1999JD901011, 2000.
- Liu, S. C., Kley, D., McFarland, M., Mahlman, J. D., and Levy, H.: On the Origin of Tropospheric Ozone, *J. Geophys. Res.-Oceans*, 85, 7546–7552, doi:10.1029/JC085iC12p07546, 1980.
- Loveland, T. R., Reed, B. C., Brown, J. F., Ohlen, D. O., Zhu, Z., Yang, L., and Merchant, J. W.: Development of a global land cover characteristics database and IGBP DIS-Cover from 1 km AVHRR data, *Int. J. Remote*, 21, 1303–1330, doi:10.1080/014311600210191, 2000.
- Mikkelsen, T. N., Ro-Poulsen, H., Pilegaard, K., Hovmand, M. F., Jensen, N. O., Christensen, C. S., and Hummelshøj, P.: Ozone uptake by an evergreen forest canopy: temporal variation and possible mechanisms, *Environ. Pollut.*, 109, 423–429, doi:10.1016/S0269-7491(00)00045-2, 2000.
- Mikkelsen, T. N., Ro-Poulsen, H., Hovmand, M. F., Jensen, N. O., Pilegaard, K., and Egelov, A. H.: Five-year measurements of ozone fluxes to a Danish Norway spruce canopy, *Atmos. Environ.*, 38, 2361–2371, doi:10.1016/j.atmosenv.2003.12.036, 2004.
- Muller, J. B. A., Percival, C. J., Gallagher, M. W., Fowler, D., Coyle, M., and Nemitz, E.: Sources of uncertainty in eddy covariance ozone flux measurements made by dry chemiluminescence fast response analysers, *Atmos. Meas. Tech.*, 3, 163–176, doi:10.5194/amt-3-163-2010, 2010.
- Munger, J. W., Wofsy, S. C., Bakwin, P. S., Fan, S. M., Goulden, M. L., Daube, B. C., Goldstein, A. H., Moore, K. E., and Fitzjarrald, D. R.: Atmospheric deposition of reactive nitrogen oxides and ozone in a temperate deciduous forest and a subarctic woodland .1. Measurements and mechanisms, *J. Geophys. Res.-Atmos.*, 101, 12639–12657, doi:10.1029/96JD00230, 1996.
- Pitari, G., Palmeri, S., Visconti, G., and Prinn, R. G.: Ozone Response To A CO<sub>2</sub> Doubling – Results From A Stratospheric Circulation Model With Heterogeneous Chemistry, *J. Geophys. Res.-Atmos.*, 97, 5953–5962, 1992.
- Prather, M. J. and Ehhalt, D.: Atmospheric Chemistry and Greenhouse Gases, in: *Climate Change 2001: The Scientific Basis*, Cambridge University Press, 2001.
- Rannik, Ü., Altimir, N., Mammarella, I., Bäck, J., Rinne, J., Ruuskanen, T. M., Hari, P., Vesala, T., and Kulmala, M.: Ozone deposition into a boreal forest over a decade of observations: evaluating deposition partitioning and driving variables, *Atmos. Chem. Phys.*, 12, 12165–12182, doi:10.5194/acp-12-12165-2012, 2012.
- Reich, P. B. and Amundson, R. G.: Ambient Levels of Ozone Reduce Net Photosynthesis In Tree and Crop Species, *Science*, 230, 566–570, doi:10.1126/science.230.4725.566, 1985.
- Rotman, D. A., Tannahill, J. R., Kinnison, D. E., Connell, P. S., Bergmann, D., Proctor, D., Rodriguez, J. M., Lin, S. J., Rood, R. B., Prather, M. J., Rasch, P. J., Considine, D. B., Ramaroson, R., and Kawa, S. R.: Global Modeling Initiative assessment model: Model description, integration, and testing of the transport shell, *J. Geophys. Res.-Atmos.*, 106, 1669–1691, doi:10.1029/2000JD900463, 2001.
- Rotman, D. A., Atherton, C. S., Bergmann, D. J., Cameron-Smith, P. J., Chuang, C. C., Connell, P. S., Dignon, J. E., Franz, A., Grant, K. E., Kinnison, D. E., Molenkamp, C. R., Proctor, D. D., and Tannahill, J. R.: IMPACT, the LLNL 3-D global atmospheric chemical transport model for the combined troposphere and stratosphere: Model description and analysis of ozone and other trace gases, *J. Geophys. Res.-Atmos.*, 109, D04303, doi:10.1029/2002JD003155, 2004.
- The Royal Society: Ground-level ozone in the 21st century: future trends, impacts and policy implications, Policy Document, 15/08, 2008.
- Rummel, U., Ammann, C., Kirkman, G. A., Moura, M. A. L., Foken, T., Andreae, M. O., and Meixner, F. X.: Seasonal variation of ozone deposition to a tropical rain forest in southwest Amazonia, *Atmos. Chem. Phys.*, 7, 5415–5435, doi:10.5194/acp-7-5415-2007, 2007.
- Sanderson, M. G., Dentener, F. J., Fiore, A. M., Cuvelier, C., Keating, T. J., Zuber, A., Atherton, C. S., Bergmann, D. J., Diehl, T., Doherty, R. M., Duncan, B. N., Hess, P., Horowitz, L. W., Jacob, D. J., Jonson, J. E., Kaminski, J. W., Lupu, A., MacKenzie, I. A., Mancini, E., Marmer, E., Park, R., Pitari, G., Prather, M. J., Pringle, K. J., Schroeder, S., Schultz, M. G., Shindell, D. T., Szopa, S., Wild, O., and Wind, P.: A multi-model study of the hemispheric transport and deposition of oxidised nitrogen, *Geophys. Res. Lett.*, 35, L17815, doi:10.1029/2008GL035389, 2008.
- Shindell, D. T., Grenfell, J. L., Rind, D., Grewe, V., and Price, C.: Chemistry-climate interactions in the Goddard Institute for Space Studies general circulation model: 1. Tropospheric chemistry model description and evaluation, *J. Geophys. Res.*, 106, 8047–8075, doi:10.1029/2000JD900704, 2001.

- Simpson, D.: Long-period Modeling of Photochemical Oxidants In Europe – Model-calculations For July 1985, *Atmos. Environ. A-Gen.*, 26, 1609–1634, doi:10.1016/0960-1686(92)90061-O, 1992.
- Simpson, D., Benedictow, A., Berge, H., Bergström, R., Emberson, L. D., Fagerli, H., Flechard, C. R., Hayman, G. D., Gauss, M., Jonson, J. E., Jenkin, M. E., Nyíri, A., Richter, C., Semeena, V. S., Tsyro, S., Tuovinen, J.-P., Valdebenito, Á., and Wind, P.: The EMEP MSC-W chemical transport model – technical description, *Atmos. Chem. Phys.*, 12, 7825–7865, doi:10.5194/acp-12-7825-2012, 2012.
- Simpson, D., Arneth, A., Mills, G., Solberg, S., and Uddling, J.: Ozone – the persistent menace: interactions with the N cycle and climate change, *Current Opinion in Environmental Sustainability*, 9–10, 9–19, doi:10.1016/j.cosust.2014.07.008, 2014.
- Sitch, S., Cox, P. M., Collins, W. J., and Huntingford, C.: Indirect radiative forcing of climate change through ozone effects on the land-carbon sink, *Nature*, 448, 791–794, doi:10.1038/nature06059, 2007.
- Stella, P., Personne, E., Loubet, B., Lamaud, E., Ceschia, E., Béziat, P., Bonnefond, J. M., Irvine, M., Keravec, P., Mascher, N., and Cellier, P.: Predicting and partitioning ozone fluxes to maize crops from sowing to harvest: the Surf atm-O<sub>3</sub> model, *Biogeosciences*, 8, 2869–2886, doi:10.5194/bg-8-2869-2011, 2011.
- Stevenson, D. S., Dentener, F. J., Schultz, M. G., Ellingsen, K., van Noije, T. P. C., Wild, O., Zeng, G., Amann, M., Atherton, C. S., Bell, N., Bergmann, D. J., Bey, I., Butler, T., Cofala, J., Collins, W. J., Derwent, R. G., Doherty, R. M., Drevet, J., Eskes, H. J., Fiore, A. M., Gauss, M., Hauglustaine, D. A., Horowitz, L. W., Isaksen, I. S. A., Krol, M. C., Lamarque, J. F., Lawrence, M. G., Montanaro, V., Müller, J. F., Pitari, G., Prather, M. J., Pyle, J. A., Rast, S., Rodriguez, J. M., Sanderson, M. G., Savage, N. H., Shindell, D. T., Strahan, S. E., Sudo, K., and Szopa, S.: Multimodel ensemble simulations of present-day and near-future tropospheric ozone, *J. Geophys. Res.-Atmos.*, 111, D08301, doi:10.1029/2005JD006338, 2006.
- Sudo, K., Takahashi, M., Kurokawa, J.-I., and Akimoto, H.: CHASER: A global chemical model of the troposphere 1. Model description, *J. Geophys. Res.*, 107, 4339–4359, doi:10.1029/2001JD001113, 2002.
- Tai, A. P. K., Martin, M. V., and Heald, C. L.: Threat to future global food security from climate change and ozone air pollution, *Nature Climate Change*, 4, 817–821, doi:10.1038/NCLIMATE2317, 2014.
- Tuovinen, J. P., Ashmore, M. R., Emberson, L. D., and Simpson, D.: Testing and improving the EMEP ozone deposition module, *Atmos. Environ.*, 38, 2373–2385, doi:10.1016/j.atmosenv.2004.01.026, 2004.
- Tuovinen, J.-P., Emberson, L., and Simpson, D.: Modelling ozone fluxes to forests for risk assessment: status and prospects, *Ann. For. Sci.*, 66, p. 401, doi:10.1051/forest/2009024, 2009.
- Val Martin, M., Heald, C. L., and Arnold, S. R.: Coupling dry deposition to vegetation phenology in the Community Earth System Model: Implications for the simulation of surface O<sub>3</sub>, *Geophys. Res. Lett.*, 41, 2988–2996, doi:10.1002/2014GL059651, 2014.
- Van Dingenen, R., Dentener, F. J., Raes, F., Krol, M. C., Emberson, L., and Cofala, J.: The global impact of ozone on agricultural crop yields under current and future air quality legislation, *Atmos. Environ.*, 43, 604–618, doi:10.1016/j.atmosenv.2008.10.033, 2009.
- Wang, Y. H., Jacob, D. J., and Logan, J. A.: Global simulation of tropospheric O<sub>3</sub>-NO<sub>x</sub>-hydrocarbon chemistry 1. Model formulation, *J. Geophys. Res.-Atmos.*, 103, 10713–10725, doi:10.1029/98JD00158, 1998.
- Wesely, M. L.: Parameterization of Surface Resistances To Gaseous Dry Deposition In Regional-scale Numerical-models, *Atmos. Environ.*, 23, 1293–1304, doi:10.1016/0004-6981(89)90153-4, 1989.
- Wesely, M. L. and Hicks, B. B.: A review of the current status of knowledge on dry deposition, *Atmos. Environ.*, 34, 2261–2282, doi:10.1016/S1352-2310(99)00467-7, 2000.
- WHO: WHO Air quality guidelines for particulate matter, ozone, nitrogen dioxide, and sulfur dioxide. Global update 2005, Summary of risk assessment, Tech. rep., World Health Organisation, WHO Press, World Health Organization, 20 Avenue Appia, 1211 Geneva 27, Switzerland, 2005.
- Wild, O.: Modelling the global tropospheric ozone budget: exploring the variability in current models, *Atmos. Chem. Phys.*, 7, 2643–2660, doi:10.5194/acp-7-2643-2007, 2007.
- Wild, O. and Prather, M. J.: Excitation of the primary tropospheric chemical mode in a global three-dimensional model, *J. Geophys. Res.*, 105, 24647–24660, doi:10.1029/2000JD900399, 2000.
- Wolfe, G. M., Thornton, J. A., McKay, M., and Goldstein, A. H.: Forest-atmosphere exchange of ozone: sensitivity to very reactive biogenic VOC emissions and implications for incanopy photochemistry, *Atmos. Chem. Phys.*, 11, 7875–7891, doi:10.5194/acp-11-7875-2011, 2011.
- Wu, S., Mickley, L. J., Kaplan, J. O., and Jacob, D. J.: Impacts of changes in land use and land cover on atmospheric chemistry and air quality over the 21st century, *Atmos. Chem. Phys.*, 12, 1597–1609, doi:10.5194/acp-12-1597-2012, 2012.
- Young, P. J., Archibald, A. T., Bowman, K. W., Lamarque, J.-F., Naik, V., Stevenson, D. S., Tilmes, S., Voulgarakis, A., Wild, O., Bergmann, D., Cameron-Smith, P., Cionni, I., Collins, W. J., Dal-søren, S. B., Doherty, R. M., Eyring, V., Faluvegi, G., Horowitz, L. W., Josse, B., Lee, Y. H., MacKenzie, I. A., Nagashima, T., Plummer, D. A., Righi, M., Rumbold, S. T., Skeie, R. B., Shindell, D. T., Strode, S. A., Sudo, K., Szopa, S., and Zeng, G.: Pre-industrial to end 21st century projections of tropospheric ozone from the Atmospheric Chemistry and Climate Model Intercomparison Project (ACCMIP), *Atmos. Chem. Phys.*, 13, 2063–2090, doi:10.5194/acp-13-2063-2013, 2013.
- Zeng, T., Wang, Y. H., Chance, K., Browell, E. V., Ridley, B. A., and Atlas, E. L.: Widespread persistent near-surface ozone depletion at northern high latitudes in spring, *Geophys. Res. Lett.*, 30, 2298, doi:10.1029/2003GL018587, 2003.
- Zhang, L. M., Moran, M. D., Makar, P. A., Brook, J. R., and Gong, S. L.: Modelling gaseous dry deposition in AURAMS: a unified regional air-quality modelling system, *Atmos. Environ.*, 36, 537–560, doi:10.1016/S1352-2310(01)00447-2, 2002.